Electron-hole excitations and optical spectra from first principles

Michael Rohlfing

Institut für Theoretische Physik II – Festkörperphysik, Universität Münster, Wilhelm-Klemm-Straße 10, 48149 Münster, Germany

Steven G. Louie

Department of Physics, University of California, Berkeley, California 94720-7300
and Materials Science Division, Lawrence Berkeley National Laboratory, Berkeley, California 94720

(Received 13 April 2000)

We present a recently developed approach to calculate electron-hole excitations and the optical spectra of condensed matter from first principles. The key concept is to describe the excitations of the electronic system by the corresponding one- and two-particle Green's function. The method combines three computational techniques. First, the electronic ground state is treated within density-functional theory. Second, the single-particle spectrum of the electrons and holes is obtained within the GW approximation to the electron self-energy operator. Finally, the electron-hole interaction is calculated and a Bethe-Salpeter equation is solved, yielding the coupled electron-hole excitations. The resulting solutions allow the calculation of the entire optical spectrum. This holds both for bound excitonic states below the band gap, as well as for the resonant spectrum above the band gap. We discuss a number of technical developments needed for the application of the method to real systems. To illustrate the approach, we discuss the excitations and optical spectra of spatially isolated systems (atoms, molecules, and semiconductor clusters) and of extended, periodic crystals (semiconductors and insulators).

I. INTRODUCTION

Optical spectra provide extremely useful ways to investigate condensed-matter systems. Absorption, reflectivity, photoluminescence, and other optical techniques are commonly used to characterize materials. In addition, optical excitations provide the basis for a vast range of technical applications, including light-emitting devices, laser technology, and photovoltaics. In this context, it is of great importance to be able to describe accurately such excitations by highly reliable and efficient *ab initio* approaches.

For more than two decades, *ab initio* techniques have been used to investigate many properties of materials. Density-functional theory (DFT) has proven to be a very powerful tool for electronic ground-state properties. For the single-particle spectrum of electrons and holes, one-body Green's function approaches based on the GW approximation[1,2] (GWA) for the electron self-energy have turned out to be highly successful.[3–5] Very accurate quasiparticle (QP) properties have been obtained by this method, with remaining uncertainties in the order of 0.1 eV, thus making the GWA a standard tool in predicting the electron quasiparticle spectra of moderately correlated materials in various situations.[3–7] However, neither the standard DFT nor GWA allows for a correct evaluation of *optical* spectra or other charge-neutral excitations. The optical spectrum calculated within the independent-quasiparticle picture often shows significant deviations from experiment (see the discussion in Sec. IV B). The energetic position of characteristic peaks can be wrong, and the amplitudes of the peaks can deviate from experiment by a factor of 2 or more. The most striking failure of the independent-particle spectrum is that it does not describe bound exciton states, which are dominant in systems of reduced dimensions.

It has long been known that the investigation of optical electron-hole excitations requires an effective two-body approach going beyond the single-particle picture of individual quasielectron and quasihole excitations,[8,9] and that the corresponding spectra can be drastically influenced by the electron-hole interaction.[10] A rigorous approach to optical spectra is given by evaluating the two-body Green's function G_2 (on the basis of the one-body Green's function G_1, which may be described by the GWA). Starting from the QP electron and hole states of G_1 and their QP energies, the electron-hole interaction, which results from the self-energy operator, have to be calculated. Thereafter, the equation of motion for G_2 (known as the Bethe-Salpeter equation) is solved, yielding the coupled, correlated electron-hole excitation states.[8–10] Together with the corresponding optical transition matrix elements that result as coherent superpositions from those of free electron-hole pairs, the entire linear optical spectrum of a material can be evaluated. The realization of this approach, however, has long been limited to rather simple situations or to simplifying model approximations due to the complicated two-particle nature of the problem.

Only recently, the development of efficient computational techniques has made it possible to investigate the optical spectra of real materials from first principles. The method we present here is an approach that allows not only the *ab initio* calculation of the optical spectrum, but also of the effective electron-hole wave functions for both bound and unbound excitonic states. It has been applied successfully to investigate the optical spectrum of semiconductor clusters, of bulk crystals, of one-dimensional polymers, and of the semiconducting Si(111)-(2×1) surface.[11] There have also been several other works in the literature on the *ab initio* calculation of optical spectra using different numerical techniques and approximations. Onida *et al.*[12] as well as Albrecht *et al.*[13]

addressed the spectrum of a small Na cluster, of the insulator Li_2O, and the semiconductors Si and diamond. Benedict *et al.*[14] calculated the optical absorption spectrum of a large number of insulators and semiconductors. van der Horst *et al.*[15] studied the spectrum of the polymer polythiophene. In all cases, the inclusion of the electron-hole interaction (i.e., excitonic effects) turns out to be crucial for arriving at a comprehensive understanding of the optical spectra and to obtain results in agreement with experimental data.

The main focus of our present paper is to discuss in detail the techniques that we used in Ref. 11 for the calculation of the optical spectra of various materials. We demonstrate how the electron-hole interaction is calculated and the resulting excitonic effects are incorporated. An important issue is that the underlying concepts can equally well be used to investigate very different materials, like small localized systems (atoms, clusters, and molecules), extended systems (such as polymers, surfaces, and crystals) and any system in between, thus covering the entire range from the atomic length scale to macroscopic materials. To illustrate this point, we discuss results for two extreme situations: for single atoms and small molecules and clusters on the one hand, and for three-dimensionally periodic crystals on the other hand. The actual treatment of excitonic effects, although they are in principle analogous for all systems, requires somewhat different techniques for the different material classes.

The paper is organized as follows. In Sec. II we give a short introduction to the many-body concepts on which our approach is based, and we outline some approximations required for the actual calculations. Section III addresses excitations in atoms, molecules, and clusters, and examines a number of practical issues related to the numerical evaluation of the approach for such systems. In Sec. IV some specific problems in dealing with extended, periodic crystals are investigated, and the optical spectra of semiconductors and insulators are presented. A short summary concludes the paper in Sec. V.

II. BASIC THEORETICAL FRAMEWORK

In this section we briefly sketch out the basic concepts of describing excitations by Green's functions. More comprehensive discussions on the formalism are given, for example, by Hedin,[1] by Hedin and Lundqvist,[2] by Sham and Rice,[8] by Strinati,[9] by Hanke and Sham,[10] and by Del Sole and Fiorino.[16]

Corresponding to the general framework, our computational approach to realize these concepts consists of three successive steps: (A) a DFT calculation for the electronic ground state, (B) a GW calculation to obtain the QP excitation spectrum of electrons and holes, and (C) the calculation of coupled electron-hole excitations and the evaluation of the optical spectrum.

A. The electronic ground state

The starting point of our approach is the calculation of the ground-state configuration $|N,0\rangle$ of the electronic subsystem of N electrons for a given atomic structure. In the present work we focus on closed-shell systems, i.e., the total spin of the ground state is zero.[17] For simplicity, the spin-orbit interaction is not taken into account in the discussion.[17] The

system should have an energy gap.[18] The ground state can be described, for instance, by density-functional theory (DFT) within the local-density approximation (LDA). Details of the method can be found elsewhere.[5] In our actual calculations of the examples described, we employ norm-conserving *ab initio* pseudopotentials[19] and Gaussian-orbital basis functions.[5] We take the atomic structure as fixed and ignore coupling of the optical excitations to the atomic geometry. Related effects such as spectral broadening, vibrational and rotational side bands, polaronic effects, self-trapping of excitons, and finite lifetimes of excitations are not considered throughout the paper.

B. Quasiparticle excitations

Based on the ground-state configuration $|N,0\rangle$, the one-body Green's function

$$G_1(1,2) = -i\langle N,0|T(\psi(1)\psi^+(2))|N,0\rangle \qquad (1)$$

describes particlelike excitation processes in which an electron is removed from the system ($N \to N-1$) or added to it ($N \to N+1$).[2] G_1 may be obtained from a Dyson-type equation of motion,

$$[H_0 + \Sigma(E)]G_1(E) = EG_1(E). \qquad (2)$$

In this equation, $H_0 = T_0 + V_{ext} + V_{Coul}$ is the Hamiltonian in the Hartree approximation. The exchange and correlation effects among the electrons are described by the electron self-energy operator $\Sigma(E)$. We calculate Σ within the GW approximation,[1,2]

$$\Sigma = iG_1W, \qquad (3)$$

i.e., Σ is given as a product of the one-particle Green's function G_1 and the screened Coulomb interaction W. G_1 and W are evaluated from the results of the underlying DFT-LDA calculation of Sec. II A, which yields wave functions $|\psi_m^{DFT}\rangle$ and energies E_m^{DFT}. W is calculated within the random-phase approximation (RPA) (for details, see Refs. 3–5). As usual, the equation of motion for G_1 is not evaluated in the general form given by Eq. (2). Instead, it is transformed into the corresponding Dyson's equation for the quasiparticles of the system, i.e., the (long-lived) QP electron and hole states:

$$[H_0 + \Sigma(E_m^{QP})]|\psi_m^{QP}\rangle = E_m^{QP}|\psi_m^{QP}\rangle. \qquad (4)$$

In practice, Eq. (4) is evaluated in the basis given by the DFT states $|\psi_m^{DFT}\rangle$. Assuming that the DFT and QP wave functions are the same (which is often the case),[3] the QP energy of a state m is given by

$$E_m^{QP} = E_m^{DFT} + \langle\psi_m|\Sigma(E_m^{QP}) - V_{xc}|\psi_m\rangle, \qquad (5)$$

where $V_{xc}(\mathbf{r})$ is the DFT exchange-correlation potential. [Equation (5) is equivalent to a first-order perturbation calculation.] If the DFT and QP wave functions are not the same, the QP states can nevertheless be expanded in the DFT states, $|\psi_m^{QP}\rangle = \Sigma_{n'}a_{n'}^{(m)}|\psi_{n'}^{DFT}\rangle$, which allows one to set up an (energy-dependent) QP Hamiltonian

$$H_{nn'}^{QP}(E) = E_n^{DFT}\delta_{nn'} + \langle\psi_n^{DFT}|\Sigma(E) - V_{xc}|\psi_{n'}^{DFT}\rangle \qquad (6)$$

From $H_{nn'}^{QP}(E)$, the QP states and energies can be obtained. Band structures and electronic spectra of many systems have been calculated within the GW approach.[3–7] In the present context, the QP band structure, i.e., the spectrum of individual electron and hole states, serves as a basis for the investigation of coupled electron-hole excitations and of the optical spectrum.

Note that, in principle, the energy-dependent character of the off-diagonal matrix elements of $H_{nn'}^{QP}(E)$, as well as the non-Hermitian character of $\Sigma(E)$, could lead to non-orthogonal QP states and thus to conceptual problems in the following studies of electron-hole excitations. In all cases studied here, however, the non-Hermitian part of Σ is small for all relevant states, and the coupling among the LDA states only involves states with energies close to each other. The violation of orthogonality is thus very small and does not affect the following investigation of the two-particle processes.

C. Electron-hole excitations

1. Electron-hole interaction and the Bethe-Salpeter equation

In this section, we discuss electron-hole excitations $|N,0\rangle \rightarrow |N,S\rangle$ that do not change the total number of N electrons. A rigorous approach to them is given by investigating the two-particle Green's function and solving its equation of motion, which is known as the Bethe-Salpeter equation (BSE). For a more detailed discussion of the formalism we refer to the work by Strinati (see Ref. 9). Here we restrict ourselves to a brief introduction and rather focus on the actual realization of the approach within an *ab initio* framework.

Following Strinati,[9] we investigate the Bethe-Salpeter equation in the form

$$L(12;1'2') = L_0(12;1'2') + \int d(3456) L_0(14;1'3)$$
$$\times K(35;46) L(62;52'). \qquad (7)$$

$L(12;1'2')$ denotes the electron-hole correlation function and $K(35;46)$ the electron-hole interaction kernel (see below). $L_0(12;1'2') = G_1(1,2') G_1(2,1')$ corresponds to free electron-hole pairs with the interaction K switched off. The set of variables (1) comprises position, spin, and time coordinates: $(1) = (\mathbf{x}_1, t_1) = (\mathbf{r}_1, \sigma_1, t_1)$. L depends on four time variables, related to two creation processes (electron and hole) and two annihilation processes. In the context of optical excitations, we restrict ourselves to *simultaneous* creation and simultaneous annihilation, so only two of the four time variables are independent.[9] Due to time homogeneity in the absence of external fields, only the difference of these two time variables is finally relevant for Eq. (7) and is used to carry out a one-dimensional time-energy Fourier transform into $L(12;1'2';\omega)$ where (1), (2) etc., now contain only position and spin degrees of freedom. All further discussion will take place in this energy space.

Assuming that the one-body Green's function G_1 is fully given by the electron and hole quasiparticles of the system, L_0 can be written as

$$L_0(12,1'2';\omega) = i \sum_{v,c} \left[\frac{\psi_c(\mathbf{x}_1) \psi_v^*(\mathbf{x}_1') \psi_v(\mathbf{x}_2) \psi_c^*(\mathbf{x}_2')}{\omega - (E_c - E_v)} \right.$$
$$\left. - \frac{\psi_v(\mathbf{x}_1) \psi_c^*(\mathbf{x}_1') \psi_c(\mathbf{x}_2) \psi_v^*(\mathbf{x}_2')}{\omega + (E_c - E_v)} \right], \qquad (8)$$

where v runs over the occupied hole states and c over the empty electron states. In the denominators, appropriate imaginary infinitesimals have to be included that are not shown here for sake of clarity.

Assuming that the electron-hole excitations are given by long-lived transitions (in an analogous way to the quasiparticle approximation for the single-particle problem of Sec. II B), the correlation function L of Eq. (7) can be written in a form similar to Eq. (8):

$$L(12,1'2';\omega) = i \sum_S \left[\frac{\chi_S(\mathbf{x}_1, \mathbf{x}_1') \chi_S^*(\mathbf{x}_2', \mathbf{x}_2)}{\omega - \Omega_S} \right.$$
$$\left. - \frac{\chi_S(\mathbf{x}_2, \mathbf{x}_2') \chi_S^*(\mathbf{x}_1', \mathbf{x}_1)}{\omega + \Omega_S} \right]. \qquad (9)$$

In this expression, S denotes the correlated electron-hole excitations of the system with the corresponding excitation energies Ω_S. The electron-hole amplitudes have the structure

$$\chi_S(\mathbf{x}, \mathbf{x}') = -\langle N,0 | \psi^\dagger(\mathbf{x}') \psi(\mathbf{x}) | N,S \rangle. \qquad (10)$$

In the actual evaluation of the BSE, we transform all quantities from the continuous position variables into the basis given by the single-particle wave functions of the electron and hole states, which can be understood as a second quantization procedure. The electron-hole amplitudes can thus be expressed in the form

$$\chi_S(\mathbf{x}, \mathbf{x}') = \sum_v^{occ} \sum_c^{empty} A_{vc}^S \psi_c(\mathbf{x}) \psi_v^*(\mathbf{x}') + B_{vc}^S \psi_v(\mathbf{x}) \psi_c^*(\mathbf{x}'). \qquad (11)$$

Note that in Eq. (11) one of the sums only runs over occupied states (v) and the other one over empty states (c). Among the product states $\psi\psi$, no combinations of two occupied or two empty states occur. This results from the specific form (8) of L_0 and of the BSE (7).

With the help of Eqs. (8), (9), and (11), the BSE (7) turns into a generalized eigenvalue problem

$$(E_c - E_v) A_{vc}^S + \sum_{v'c'} K_{vc,v'c'}^{AA}(\Omega_S) A_{v'c'}^S$$

$$+ \sum_{v'c'} K_{vc,v'c'}^{AB}(\Omega_S) B_{v'c'}^S = \Omega_S A_{vc}^S,$$

$$\sum_{v'c'} K_{vc,v'c'}^{BA}(\Omega_S) A_{v'c'}^S + (E_c - E_v) B_{vc}^S$$

$$+ \sum_{v'c'} K_{vc,v'c'}^{BB}(\Omega_S) B_{v'c'}^S = -\Omega_S B_{vc}^S. \qquad (12)$$

The matrix elements of the electron-hole interaction kernel K are given by

$$K^{AA}_{vc,v'c'}(\Omega_S) = i \int d(3456) \psi_v(\mathbf{x}_4) \psi_c^*(\mathbf{x}_3) K(35,46;\Omega_S)$$

$$\times \psi_{v'}^*(\mathbf{x}_5) \psi_{c'}(\mathbf{x}_6), \tag{13}$$

$$K^{AB}_{vc,v'c'}(\Omega_S) = i \int d(3456) \psi_v(\mathbf{x}_4) \psi_c^*(\mathbf{x}_3) K(35,46;\Omega_S)$$

$$\times \psi_{v'}^*(\mathbf{x}_6) \psi_{c'}(\mathbf{x}_5), \tag{14}$$

and similar expressions for K^{BA} and K^{BB}.

The above equation (12) has a block-matrix structure. The diagonal blocks are given by the energy differences ($E_c - E_v$) and the interaction matrix elements K^{AA} and K^{BB}, respectively. The off-diagonal blocks are given by K^{AB} and K^{BA}. For the systems studied here, however, the off-diagonal blocks are found to be small and have nearly no effect on the excitation energies.[20] We have calculated the excitation energies of the SiH_4 molecule with and without the off-diagonal blocks and found that the excitation energies agree with each other to within 0.03 eV (see Sec. III C). Albrecht et al.[13] have carefully investigated the influence of the off-diagonal blocks on the optical spectrum of bulk Si and found nearly no effect for the absorption spectrum. [Some other optical properties, however, like the macroscopic dielectric constant, may be slightly influenced by K^{AB} and K^{BA} (see Ref. 13).] Therefore we set $K^{AB} = K^{BA} = 0$, which decouples Eq. (12) into two equations for A^S_{vc} and B^S_{vc} separately, and both equations yield exactly the same excitations (with the only difference that for the solutions for B the excitation energies have negative sign). The positive solutions result from the eigenvalue problem

$$(E_c - E_v) A^S_{vc} + \sum_{v'c'} K^{AA}_{vc,v'c'}(\Omega_S) A^S_{v'c'} = \Omega_S A^S_{vc}. \tag{15}$$

This is equivalent to expanding the excited states in electron-hole pair configurations as

$$|N,S\rangle = \sum_v^{\text{hole}} \sum_c^{\text{elec}} A^S_{vc} \hat{a}_v^\dagger \hat{b}_c^\dagger |N,0\rangle =: \sum_v^{\text{hole}} \sum_c^{\text{elec}} A^S_{vc} |vc\rangle, \tag{16}$$

where $\hat{a}_v^\dagger$ and $\hat{b}_c^\dagger$ create a hole or an electron, respectively, to the many-body ground state $|N,0\rangle$. The expansion of Eq. (16) is also known as the Tamm-Dancoff approximation.[14,21]

The electron-hole interaction kernel K is given by the functional derivative

$$K(35;46) = \frac{\delta[V_{\text{Coul}}(3)\delta(3,4) + \Sigma(3,4)]}{\delta G_1(6,5)}. \tag{17}$$

In order to be consistent with the QP band-structure calculation, we again employ the GW approximation for the self-energy operator Σ. Under the additional assumption that the derivative of the screened interaction W with respect to G_1 can be neglected,[22] one obtains

$$K(35;46) = -i\delta(3,4)\delta(5^-,6)v(3,6)$$

$$+ i\delta(3,6)\delta(4,5)W(3^+,4) \tag{18}$$

$$=: K^x(35;46) + K^d(35;46). \tag{19}$$

The term K^x, which results from the Coulomb potential in Eq. (17), is usually called the *exchange term* while the term K^d, which results from the screened-exchange self-energy in Eq. (17), has the form of a *direct* interaction term. We will keep to this conventional terminology throughout the paper. The direct interaction term $K^d(35;46)$ is responsible for the attractive nature of the electron-hole interaction and the formation of bound electron-hole states (i.e., excitons). The exchange interaction term $K^x(35;46)$, on the other hand, controls details of the excitation spectrum, such as the splitting between spin-singlet and spin-triplet excitations, or the transverse-longitudinal splitting of the s excitons in zinc-blende-structured semiconductors. Note that $K^d(35;46)$ involves the screened Coulomb interaction W while $K^x(35;46)$ contains the bare Coulomb interaction v.

The matrix elements of the interaction are given by

$$\langle vc|K^{AA,d}(\Omega_S)|v'c'\rangle$$

$$= \int d\mathbf{x}\, d\mathbf{x}'\, \psi_c^*(\mathbf{x}) \psi_{c'}(\mathbf{x}) \psi_v(\mathbf{x}') \psi_{v'}^*(\mathbf{x}')$$

$$\times \frac{i}{2\pi} \int d\omega\, e^{-i\omega 0^+} W(\mathbf{r},\mathbf{r}',\omega)$$

$$\times \left[\frac{1}{\Omega_S - \omega - (E_{c'}^{\text{QP}} - E_v^{\text{QP}}) + i0^+} \right.$$

$$\left. + \frac{1}{\Omega_S + \omega - (E_c^{\text{QP}} - E_v^{\text{QP}}) + i0^+} \right] \tag{20}$$

and

$$\langle vc|K^{AA,x}|v'c'\rangle = \int d\mathbf{x}\, d\mathbf{x}'\, \psi_c^*(\mathbf{x}) \psi_v(\mathbf{x}) v(\mathbf{r},\mathbf{r}')$$

$$\times \psi_{c'}(\mathbf{x}') \psi_{v'}^*(\mathbf{x}'). \tag{21}$$

The matrix elements consist of six-dimensional real-space integrals, involving the QP electron and hole wave functions. Although the evaluation of these integrals is straightforward, the details of the electronic system under investigation will require specific techniques to calculate the terms (20) and (21) (see Secs. III and IV).

In addition to the real-space integration, the direct interaction term $K^d(35;46)$ requires a frequency integration. We evaluate this by expanding the screened interaction in the same plasmon-pole model which is employed in the GW part of our approach (for details, see Ref. 5), which can be written as

$$W(\mathbf{r},\mathbf{r}',\omega) = \sum_l W_l(\mathbf{r},\mathbf{r}') \frac{\omega_l}{2}$$

$$\times \left(\frac{1}{\omega - \omega_l + i0^+} - \frac{1}{\omega + \omega_l - i0^+} \right), \tag{22}$$

where ω_l denotes the plasmon frequency and $W_l(\mathbf{r},\mathbf{r}')$ the spatial behavior of the plasmon mode l. This allows one to carry out the frequency integration analytically:

$$\langle vc|K^{AA,d}(\Omega_S)|v'c'\rangle = -\sum_l \int d\mathbf{x}\, d\mathbf{x}'\, \psi_c^*(\mathbf{x})\psi_{c'}(\mathbf{x})\psi_v(\mathbf{x}')\psi_{v'}^*(\mathbf{x}')W_l(\mathbf{r},\mathbf{r}')$$

$$\times \frac{\omega_l}{2}\left[\frac{1}{\omega_l-(\Omega_S-(E_{c'}^{QP}-E_v^{QP}))}+\frac{1}{\omega_l-(\Omega_S-(E_c^{QP}-E_v^{QP}))}\right]. \tag{23}$$

In many cases (e.g., in most semiconductor crystals), the excitations $|S\rangle$ are mainly composed from electron-hole pair configurations $|vc\rangle$ whose transition energies $(E_c^{QP}-E_v^{QP})$ are close to the resulting excitation energy Ω_S, i.e., the relevant differences $\Omega_S-(E_c^{QP}-E_v^{QP})$ are much smaller than the plasmon energies ω_l that control the dynamics of the screening. In such a case, Eq. (23) can be replaced by the simple result

$$\langle vc|K^{AA,d}|v'c'\rangle$$

$$= -\int d\mathbf{x}\, d\mathbf{x}'\, \psi_c^*(\mathbf{x})\psi_{c'}(\mathbf{x})\psi_v(\mathbf{x}')$$

$$\times \psi_{v'}^*(\mathbf{x}')W(\mathbf{r},\mathbf{r}',\omega=0), \tag{24}$$

which fully ignores the dynamical properties of W. In other cases, however, the differences $\Omega_S-(E_c^{QP}-E_v^{QP})$ may be larger (as, e.g., in atoms and molecules). This happens, e.g., if the excitonic binding energies are of the same order of magnitude as the characteristic plasmon frequencies ω_l or if the excitations $|S\rangle$ are composed from free electron-hole transitions with very different transition energies $(E_c^{QP}-E_v^{QP})$. In such cases the simple result of Eq. (24) may not hold and the electron-hole interaction has to be evaluated as in Eq. (23). Note that the interaction term in Eq. (23) depends on Ω_S. This poses a significant problem since it re-

quires calculating the interaction and solving the BSE self-consistently. We do this by an iterative procedure. In the first step, we ignore the dynamics of W and employ static screening [i.e., K^d is taken from Eq. (24)]. The BSE is solved, yielding the excited states $|S\rangle$ and a first estimate of their excitation energies $\Omega_S^{(0)}$. Thereafter, K^d is calculated again [employing $\Omega_S^{(0)}$ in Eq. (23)]. The difference between the updated K^d and the originally used $K^{d,0}$ is taken as a perturbation and treated in first order, thus updating Ω_S (the composition of the excited state $|S\rangle$ is not changed). The procedure may be repeated several times until Ω_S reaches convergence (typically after 2–3 iterations).

An important issue concerns the spin structure of the solutions of the BSE. Depending on the strength of the spin-orbit interaction in the system, two situations can occur: If the spin-orbit interaction is negligible (i.e., as compared to the electron-hole interaction), the single-particle states (v and c) can be classified as spin-up states ($v\uparrow$ and $c\uparrow$) and spin-down states ($v\downarrow$ and $c\downarrow$). (Note that for occupied states v, this spin corresponds to the *electron* that originally occupies the state. The spin of the corresponding *hole* would be the negative.) The Hilbert space of the electron-hole pairs (vc) now consists of four subspaces: $v\uparrow c\uparrow$, $v\uparrow c\downarrow$, $v\downarrow c\uparrow$, and $v\downarrow c\downarrow$. Between these subspaces, most of the matrix elements of Eqs. (20) and (21) are zero; in the notation of these subspaces the BSE Hamiltonian obtains the form

$$H^{eh}=\begin{pmatrix} D+K^d+K^x & 0 & 0 & K^x \\ 0 & D+K^d & 0 & 0 \\ 0 & 0 & D+K^d & 0 \\ K^x & 0 & 0 & D+K^d+K^x \end{pmatrix}\begin{matrix}(\leftrightarrow v\uparrow c\uparrow)\\(\leftrightarrow v\uparrow c\downarrow)\\(\leftrightarrow v\downarrow c\uparrow)\\(\leftrightarrow v\downarrow c\downarrow)\end{matrix}, \tag{25}$$

with $D \hat{=} (E_c-E_v)$. This Hamiltonian decouples into a spin-triplet class of solutions [consisting of the subspaces $v\uparrow c\downarrow$, $v\downarrow c\uparrow$, and $(1/\sqrt{2})(v\uparrow c\uparrow+v\downarrow c\downarrow)$], for which the Hamiltonian becomes $D+K^d$, and a spin-singlet class of solutions [consisting of the subspace $(1/\sqrt{2})(v\uparrow c\uparrow-v\downarrow c\downarrow)$], for which the Hamiltonian becomes $D+K^d+2K^x$. The BSE can thus be solved for singlet and triplet configurations separately. The spin degrees of freedom have been completely eliminated from the remaining problem.

If the spin-orbit interaction is of the same order of magnitude as the electron-hole interaction or larger, the single-particle states cannot be classified as spin-up and spin-down

states. In the electron-hole excitations, singlet and triplet configurations are mixed and the BSE Hamiltonian must be discussed including its full spin structure (see, for example, our results for GaAs in Ref. 11). Since this increases the number of basis states by a factor of 4, the evaluation of the BSE becomes more difficult. More complex spin structures are also found for open-shell systems that do not have a spin-singlet ground state.

2. Optical spectrum

The most important measurable quantity we address in this paper is the interaction of an external light field with excitations in the system. This is described by the macroscopic transverse dielectric function $\epsilon(\omega)$ of the system,

which corresponds to the current-current correlation function.[23] We calculate its imaginary part $\epsilon_2(\omega)$ as

$$\epsilon_2(\omega) = \frac{16\pi e^2}{\omega^2} \sum_S |\vec{\lambda} \cdot \langle 0|\vec{v}|S\rangle|^2 \delta(\omega - \Omega_S), \quad (26)$$

where $\vec{\lambda} = \vec{A}/|\vec{A}|$ is the polarization vector of the light and $\vec{v} = i/\hbar[H,\vec{r}]$ is the single-particle velocity operator (which corresponds to the current operator).

The careful calculation of the optical transition matrix elements $\langle 0|\vec{v}|S\rangle$ is crucial. Without the electron-hole interaction, the excitations are given by vertical transitions between independent hole and electron states, and Eq. (26) reduces to the well-known expression

$$\epsilon_2^{(0)}(\omega) = \frac{16\pi e^2}{\omega^2} \sum_{v,c} |\vec{\lambda} \cdot \langle v|\vec{v}|c\rangle|^2 \delta(\omega - (E_c - E_v)), \quad (27)$$

where v (c) denotes valence (conduction) states. One main effect of the electron-hole interaction is the coupling of different electron-hole configurations $|vc\rangle$ in the excitations $|S\rangle$ [see Eq. (16)]. Concomitantly, the optical transition matrix elements are given by

$$\langle 0|\vec{v}|S\rangle = \sum_v^{\text{hole}} \sum_c^{\text{elec}} A_{vc}^S \langle v|\vec{v}|c\rangle, \quad (28)$$

i.e., by a coherent sum of the transition matrix elements of the contributing electron-hole pair configurations, including the coupling coefficients A_{vc}^S. In this context, the *phases* of the single-particle states v and c and of the coefficients A_{vc}^S are extremely important to correctly describe the interference effects in the matrix elements. It is therefore crucial that all phases are treated consistently in the wave functions, in the electron-hole interaction, and in the coupling coefficients (see also the discussion in Sec. IV).

In the calculation of $\epsilon(\omega)$, local fields, i.e., response fields of the crystal that tend to screen the electric field, play an important role. They can cause a significant reduction of the dielectric function. Within the independent-particle picture, local fields are often included by calculating the entire dielectric *matrix* $\epsilon_{\mathbf{G},\mathbf{G}'}(\omega)$ (with $\mathbf{G}$ denoting the reciprocal-lattice vectors) and evaluating the macroscopic dielectric function from the head of the inverse matrix, $\epsilon_{\mathbf{G},\mathbf{G}'}^{-1}(\omega)$. In the present context, however, this procedure is not necessary. It has been shown by Del Sole and Fiorino *et al.* that the dielectric function as given by Eq. (26) already includes the local-field effects due to the exchange term of the electron-hole interaction (for details, see Ref. 16), i.e., Eq. (26) is fully sufficient and the entire dielectric matrix $\epsilon_{\mathbf{G},\mathbf{G}'}(\omega)$ needs not to be computed.

The calculation of the transition matrix elements $\langle v|\vec{v}|c\rangle$ deserves particular attention when pseudopotentials are used. The current operator is given as $\vec{v} = i[H,\vec{r}]$. If the crystal potential is a local operator, i.e., if the potential commutes with the position operator ($[V(\vec{r}),\vec{r}]=0$), the velocity operator can be replaced by the momentum operator $\vec{p}$. In the present case of nonlocal pseudopotentials, this no longer holds and the commutator $[V(\vec{r}),\vec{r}]$ has to be accounted for:

$$\langle v|\vec{v}|c\rangle = \langle v|\vec{p} + i[V_{\text{ps}},\vec{r}]|c\rangle. \quad (29)$$

Another problem arises from the QP corrections due to the self-energy operator, which is nonlocal as well, so it does not commute with the position operator, either. Even if the QP shifts are the same for all empty states, the self-energy operator is nonlocal due to the different spatial properties of wave functions at different wave vectors. As was discussed by Levine and Allan,[24] the QP shift between the LDA and QP transition energy of an electron-hole pair $|vc\rangle$ leads to a renormalization of the optical transition matrix element:

$$\langle v|\vec{v}|c\rangle^{[\text{QP}]} := \frac{E_c^{\text{QP}} - E_v^{\text{QP}}}{E_c^{\text{LDA}} - E_v^{\text{LDA}}} \langle v|\vec{v}|c\rangle^{[\text{LDA}]}. \quad (30)$$

The effect of this renormalization is that, taking into account the division by ω^2 in Eq. (26), the weight of a transition $|vc\rangle$ in ϵ_2 is not changed when the transition is shifted to higher energies by the QP correction.

In crystals, an alternative approach, which accounts for both the nonlocal pseudopotential and the QP renormalization effects automatically, is to calculate the optical transition matix elements by $\mathbf{k} \cdot \mathbf{p}$ perturbation theory. This leads immediately to

$$\langle v\mathbf{k}|v_\alpha|c\mathbf{k}\rangle^{[\text{QP}]} = \frac{E_{c\mathbf{k}}^{\text{QP}} - E_{v\mathbf{k}}^{\text{QP}}}{q} \int \psi_{v\mathbf{k}}(\mathbf{x}) e^{-iqr_\alpha} \psi_{c,\mathbf{k}+q\mathbf{e}_\alpha}(\mathbf{x}) d\mathbf{x}, \quad (31)$$

with q being a small but finite shift to $\mathbf{k}$ in reciprocal space. To this end, the wave functions at the shifted wave vectors $\mathbf{k} + q\mathbf{e}_\alpha$ ($\alpha = x, y, z$) have to be calculated explicitly.

Another issue in the discussion of the dielectric function concerns the block-matrix structure of the BSE, as discussed in Eq. (12). It has been shown by Albrecht *et al.*[13] that the nondiagonal blocks K^{AB} and K^{BA} have nearly no effect on the $\epsilon_2(\omega)$ spectrum of semiconductors. In addition, we have found that the nondiagonal blocks have nearly no effect on the excitation energies of small atomic clusters, either (see Sec. III C). Since in the present paper we are mainly interested in absorption spectra, we set these blocks to zero and only work in the subspace of positive excitation energies. Albrecht *et al.*[13] have found, however, that the blocks do change the macroscopic dielectric constant $\epsilon_1(\omega=0)$ by up to 4% for Si. For a highly accurate calculation of $\epsilon_1(\omega=0)$, it may thus be necessary to include the off-diagonal blocks.

D. Basis sets

For the real-space representation of the single-particle wave functions $\psi_{m\mathbf{k}}(\mathbf{r})$ (within DFT, GWA, and BSE) and of the two-point functions $\epsilon(\mathbf{r},\mathbf{r}')$, $W(\mathbf{r},\mathbf{r}')$, etc. (for the GWA and BSE), basis sets are required. The bases for the wave functions and for two-point functions can be chosen independently. The most common representation is a plane-wave expansion of all functions.[3,4] Different from this, real-space representations are used by Benedict *et al.* for the BSE,[14] by Rojas *et al.* and Rieger *et al.* for the GWA,[25] and by van der

Horst *et al.* for the BSE.[15] In addition, Aryasetiawan and Gunnarsson employ linear combination of muffin-tin orbital (LMTO) bases for the DFT and the corresponding product basis for the GWA.[6]

In the current work, we employ basis sets of localized Gaussian orbitals centered at the atomic positions for both the wave functions and for all two-point functions (for details, see Ref. 5). For the extended crystals, the computational demand is about the same for Gaussian-orbital basis sets and for plane-wave calculations. For the isolated atoms and clusters, on the other hand, the use of Gaussians can be extremely advantageous due to much smaller basis sizes.

Note that, in the BSE, the basis is only necessary for the evaluation of the electron-hole interaction matrix elements. The BSE itself is treated in the basis given by the single-particle states (i.e., products of electron and hole states), which is independent of the basis representation of the wave functions. It is, however, also possible to address the BSE in a localized basis set of, e.g., atomic orbitals (see the discussion by Hanke and Sham in Ref. 10), which allows the evaluations of the optical spectrum but does not easily yield individual states $|S\rangle$.

III. ATOMS, MOLECULES, AND CLUSTERS

In this section, we investigate the excitation spectrum of small isolated systems since optical excitations of atoms, molecules, and clusters are of great importance in laser devices, dye chemicals, photochemical reactions, and many other applications. Isolated systems are often described by quantum chemistry techniques such as coupled-cluster (CC) or configuration-interaction (CI) methods. These approaches yield highly accurate results; however, they are difficult to apply to larger molecules due to their scaling behavior as $O(N^{5-7})$, where N is the number of electrons. Our present Green's function approach (GW+BSE) reaches a high degree of accuracy (~ 0.1 eV) while offering a much better scaling $[O(N^{3-4})]$. Alternative approaches to small systems would be those based on time-dependent density-functional theory (TDDFT).[26,27] Before discussing some illustrative results, some remarks on technical specifications are necessary.

A. Technical details

In the context of traditional solid-state methods, atoms, clusters, and molecules require special handling due to their spatial isolation. The most convenient approach is to put them in a supercell of sufficient size, which allows one to employ conventional techniques developed for periodic systems. The dependence of the results on the supercell size, however, has to be checked carefully. Particular attention has to be paid to artificial Coulomb interactions between the objects in different supercells. Already within DFT, additional charges on the system or permanent dipoles can lead to long-range interactions that die off very slowly with respect to the supercell size. In the GW approximation, the situation is even worse since nonphysical dynamic dipole-dipole interactions between the supercells can occur even for systems without permanent dipoles. Therefore the convergence of GW calculations for atoms and clusters with respect to supercell size can be very slow (see, e.g., the discussion by Onida *et al.* in Ref. 12).

Following Onida *et al.*,[12] we employ a natural way to overcome these problems: we truncate the Coulomb interaction $v(\mathbf{r},\mathbf{r}')=e^2/|\mathbf{r}-\mathbf{r}'|$ in real space at a radius r_c, i.e., $v(\mathbf{r},\mathbf{r}')$ is replaced by $v_c(\mathbf{r},\mathbf{r}')=(e^2/|\mathbf{r}-\mathbf{r}'|)\Theta(r_c-|\mathbf{r}-\mathbf{r}'|)$. The truncation radius r_c has to be chosen properly. In order to eliminate interaction between systems in neighboring supercells, r_c must be smaller than the supercell dimension R minus the maximum diameter d_{max} of the molecule: $r_c < R - d_{max}$. On the other hand, r_c must be larger than d_{max} itself in order not to truncate the interaction within the system: $r_c > d_{max}$. This requires that the supercell be at least twice as large in every direction as the system itself: $R > 2d_{max}$. In reciprocal space the truncation of the Coulomb interaction simply leads to $v_c(q)=(4\pi e^2/V)(1/q^2)[1-\cos(qr_c)]$. For $q \to 0$ this expression has the finite limit $v_c(0)=(4\pi e^2/V)(r_c^2/2)$.

No **k**-point sampling is required for the wave functions of finite systems. In the GW calculation, however, the evaluation of the self-energy requires a Coulomb-interaction integration, which is most conveniently carried out in reciprocal space on a grid. Depending on the required grid density, it may be necessary to sample the Brillouin zone with more than just one **k** point. However, if the Coulomb interaction is truncated and thus smoothed in reciprocal space, and if the supercell is sufficiently large, the sampling can be restricted to only the Γ point of each Brillouin zone. The other parameter of the sampling is the maximum radius in reciprocal space, or the corresponding cutoff energy. This is determined by the degree of localization of the electron and hole states.

As mentioned in Sec. II D, the matrix elements of the electron-hole interaction are calculated with Gaussian-orbital basis sets both for the wave functions and for the two-point (screened or unscreened) interaction kernel. Due to the small number of basis functions involved, these calculations are much faster than within a plane-wave basis set. Nevertheless, the limited number of basis functions can cause slight inaccuracies, in particular for the unscreened contribution to the diagonal matrix elements $[(vc)=(v'c')]$ of the electron-hole interaction. Since these contributions account for most of the interaction, a very accurate evaluation is required here. This is easily achieved by a plane-wave summation in reciprocal space, where the Coulomb interaction is diagonal:

$$\int d\mathbf{x}\, d\mathbf{x}'\, \psi_c^*(\mathbf{x})\psi_c(\mathbf{x})v_c(\mathbf{r},\mathbf{r}')\psi_v(\mathbf{x}')\psi_v^*(\mathbf{x}')$$

$$=\sum_{\mathbf{G}} \rho_{c,c}(\mathbf{G})v_c(\mathbf{G})\rho_{v,v}^*(\mathbf{G}), \tag{32}$$

where $\rho_{m,n}(\mathbf{G})=\int d\mathbf{x}\,\psi_m^*(\mathbf{x})\psi_n(\mathbf{x})e^{-i\mathbf{G}\cdot\mathbf{r}}$ is the spatial Fourier transform of a product of two wave functions. A similar formula holds for the exchange term of the electron-hole interaction. The large sum over $\mathbf{G}$ vectors is very demanding. However, since we do this only for the bare Coulomb interaction (which is diagonal in reciprocal space) and only for the diagonal matrix elements of K^{eh} $[(vc)=(v'c')]$, the computational cost is affordable. All off-diagonal matrix elements of K^{eh}, as well as the contribution of the screening to $K^{eh,d}$, are calculated with the Gaussian-orbital representation of the interaction (for details, see Ref. 5).

TABLE I. Calculated ionization energies I and first neutral excitation energies (eV) (E_S for singlet and E_T for triplet excitations) for various noble-gas atoms (in eV), compared with experimental data from Ref. 29.

		This work	Expt. (Ref. 29)
He:	I	24.68	24.586
	E_S	20.75	20.615
	E_T	19.81	19.818
Ne:	I	21.47	21.564
	E_S	16.95	16.848
	E_T	16.71	16.668
Ar:	I	15.94	15.759
	E_S	11.99	11.827
	E_T	11.76	11.631

TABLE II. Calculated HOMO energy ($\hat{=}$ negative of the ionization energy), LUMO energy ($\hat{=}$ negative of the electron affinity), lowest excitation energies (E_S for singlet, E_T for triplet excitations), and excitonic binding energies (E_B) of SiH_4 (see text), all in eV. The experimental data are from Ref. 30.

$(\Sigma - V_{xc})_{nn'}$	LDA	HF diag.	GWA/BSE diag.	GWA/BSE full	Expt.
HOMO	−8.42	−12.98	−12.69	−12.69	−12.6
LUMO	−0.57	1.49	1.10	0.27	
QP gap	7.85	14.47	13.79	12.96	
E_S		8.82	8.49	9.16	8.8
$E_{B,S}$		5.65	5.30	3.80	
E_T		7.26	7.12	8.51	
$E_{B,T}$		7.21	6.67	4.45	

B. Noble-gas atoms

The easiest systems to study are atoms. GW calculations for atoms have already been presented by Shirley and Martin.[28] The excitation spectra of atoms can be measured with extreme accuracy, allowing for a very careful check of the reliability of our method. As an illustration, Table I shows calculated results for the noble-gas atoms He, Ne, and Ar in comparison with measured data.[29] The ionization potential I is given by the negative of the QP energy of the highest occupied atomic level ($1s$, $2p$, and $3p$, respectively). The excitation energies refer to the transitions $1s^2 \rightarrow 1s^1 2s^1$ (He), $\ldots 2p^6 \rightarrow 2p^5 3s^1$ (Ne), and $\ldots 3p^6 \rightarrow 3p^5 4s^1$ (Ar), respectively. These excitations occur both as spin-singlet and as spin-triplet transitions. The excitation energies of the spin-singlet transitions are higher since they include the repulsive exchange term in the electron-hole interaction. For all ionization and excitation energies, our results show very good agreement with the measured data. The remaining differences are in the order of only 0.1 eV, which we consider the general accuracy available within the GW + BSE method.

C. Molecules

We take SiH_4 as an example to carefully discuss a number of details in the calculation of molecular spectra. This discussion applies in a very general way to many other systems. We focus on the following quantities: the ionization potential I, the electron affinity A, the lowest spin-singlet and -triplet excitation energies E_S and E_T and the corresponding excitonic binding energies (i.e., the difference between E_S (or E_T) and the QP gap, $E_{gap}^{QP} = E_{LUMO}^{QP} - E_{HOMO}^{QP}$). The results are compiled in Table II.

The first column contains the LDA highest occupied molecular orbital (HOMO) and lowest unoccupied molecular orbital (LUMO) energies (Kohn-Sham eigenvalues). The HOMO-LUMO gap amounts to 7.85 eV. The second column contains data that have been calculated within GW+BSE, but with the screening set to zero (i.e., $W \equiv v$). This is equivalent to the Hartree-Fock (HF) approximation for the self-energy operator. Compared to the LDA data, the HOMO state is significantly lowered (by more than 4 eV) while the

LUMO state is raised by 2 eV. The HF QP gap amounts to 14.5 eV. The electron-hole excitation energies, on the other hand, are 8.82 eV and 7.26 eV for the lowest spin-singlet and -triplet transition, respectively, which is in the order of magnitude of the LDA HOMO-LUMO gap. The excitonic binding energies (defined as the difference between the excitation energy and the QP gap) of 5.6 eV and 7.2 eV are very large, compared to crystalline systems. This is a consequence of the spatial confinement, which enhances the overlap between the electron and hole wave functions and thus the interaction between them.

The third column shows the corresponding results with the screening included in the self-energy operator and in the electron-hole interaction. Due to the screening, the HOMO is raised by 0.3 eV and the LUMO lowered by 0.4 eV. The excitonic binding energies are reduced by 0.3–0.5 eV. These modifications are much less pronounced than in crystalline semiconductors, where the screening changes the QP energies by several eV. This is due to the much weaker dielectric screening in small molecules. Nevertheless, the changes (several tenths of an eV) are significant, i.e., to obtain accurate results it is crucial to correctly include the screening effects, as it is done by the GW self-energy operator.

Note that for the second and third column, the QP states were taken to be those of the LDA wave functions and only the diagonal terms of $(\Sigma - V_{xc})_{nn'}$ were examined [cf. Eq. (5)]. In the small systems studied here, however, the QP wave functions of the HOMO and LUMO states and their energies must be investigated more carefully. This is shown
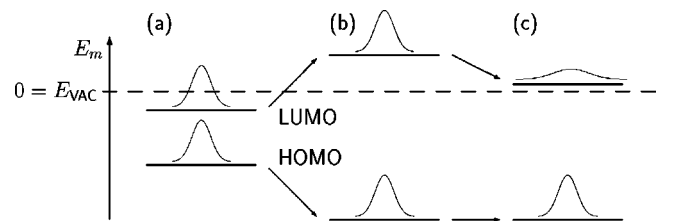

FIG. 1. Illustration of a typical single-particle spectrum and wave functions in atoms and molecules, as resulting from LDA and GW calculations (see text). (a) indicates LDA, (b) indicates first-order perturbative GWA [see Eq. (5)], and (c) refers to full diagonalization of the GW Hamiltonian [see Eq. (6)].

in column 4 of Table II and is schematically illustrated in Fig. 1. Within LDA [see panel (a)], the LUMO energy is below the vacuum level ($\equiv 0$ eV), i.e., the state is bound. Its wave function [indicated in panel (a)] is that of a localized, bound state. Within GWA, however, the LUMO state observes a strongly positive QP shift that pushes the LUMO state *above* the vacuum level [see panel (b)]. For SiH_4, the first-order perturbation evaluation of $(\Sigma - V_{xc})$ [Eq. (5)] yields a QP correction of 1.7 eV, resulting in a QP LUMO energy of 1.10 eV. Being above the vacuum level, the LUMO state is no longer bound. Therefore its wave function should be more delocalized than that of the original LDA LUMO state. This tendency of delocalization [shown in panel (c)] is described by the off-diagonal matrix elements of $(\Sigma - V_{xc})$ that control the mixing of the states when going from LDA to GWA [cf. Eq. (6)]. The LUMO state becomes more delocalized while its energy is reduced to 0.27 eV. Note that in principle, if a bound empty state does not exist, the lowest-energy state should have zero energy and be infinitely delocalized. Due to the finite basis set in representing the wave functions, however, an infinite delocalization of the LUMO is not possible and the energy remains positive. It is also interesting to note that the mixing of wave functions when including $(\Sigma - V_{xc})$ only affects the empty states. The occupied states remain nearly unchanged, i.e., the off-diagonal matrix elements of $(\Sigma - V_{xc})$ among the occupied states, as well as those between occupied and empty states, are very close to zero. This is related to the fact that the states are correctly described as bound, localized wave functions already within LDA. We have found similar behavior in many molecules, i.e., the occupied wave functions are described correctly by LDA while the LUMO state is (physically incorrectly) given by a bound state that is then turned into an unbound, delocalized state by the self-energy operator. Note that similar modifications could, in principle, also occur among the occupied states if they were incorrectly described by LDA. This could happen, e.g., in more strongly correlated systems like transition metal oxides.

The positive energy of the LUMO state (i.e., negative value of the electron affinity) means that a negative charging of the molecule is unfavorable; an additional electron will not be bound but will spontaneously separate from the molecule. In fact, to our knowledge, SiH_4^- ions have never been observed in experiment. This situation, i.e., that the LUMO state is bound in the LDA spectrum but unbound in GWA, occurs in many atoms and molecules. Therefore, a careful calculation of its wave function, including the off-diagonal matrix elements of $(\Sigma - V_{xc})$, is mandatory. We note in passing that the unbound character of the LUMO state also results from change in self-consistent field (ΔSCF) calculations within LDA total-energy approaches.

The delocalization of the empty states has a strong effect on the electron-hole interaction (see column 4 of Table II). Since the interaction depends on the overlap between the QP states, the delocalization *reduces* the interaction and leads to smaller excitonic binding energies than before. In fact, this overcompensates the lowering of the empty states by the delocalization, such that the resulting excitation energies are *higher* than before. This holds in particular for the spin-triplet excitations, thus reducing the singlet-triplet splitting of the lowest excitation in SiH_4 from 1.37 eV to 0.65 eV.

TABLE III. Excitation energies of SiH_4, calculated with different approximations to the electron-hole interaction (see text).

$K^{A,A}$	diag.	full	full	full
$K^{A,B}$	$:=0$	$:=0$	$:=0$	included
Screening	static	static	dyn.	dyn.
E_S	9.65	9.24	9.16	9.16
$E_{B,S}$	3.31	3.72	3.80	3.80
E_T	9.25	8.64	8.51	8.48
$E_{B,T}$	3.71	4.32	4.45	4.48

In Table III the effects of various simplifications of the electron-hole interaction kernel on the excitation energies and excitonic binding energies are discussed. In the first column, only the diagonal matrix elements of the interaction ($v = v'$ and $c = c'$) are taken into account. The electron-hole excitations are thus given by the free electron-hole pairs of the molecules, and the excitation energy is given by the QP gap minus the expectation value of the interaction. Excitonic coupling between different electron-hole pair configurations is completely neglected. In the second column this coupling is included by taking the off-diagonal matrix elements between the electron-hole pair configurations into account. This lowers the excitation energies by as much as 0.7 eV for the triplet state, thus demonstrating the importance of excitonic coupling for obtaining an accurate spectrum.

For the first and second columns of Table III, the electron-hole interaction has been calculated from static screening. As discussed in Sec. II C, this may not be accurate enough if the excitonic binding energies are comparable to the characteristic plasmon frequencies of the system. The dynamics of the screening can be incorporated perturbatively. The results are displayed in the third column (which is identical to the fourth column of Table II). It turns out that dynamic screening lowers the excitation energies by about 0.1 eV.

Up to now, the off-diagonal blocks $K^{A,B}$ and $K^{B,A}$ that couple negative and positive excitation frequencies have been ignored. In column 4 of Table III, we show the lowest-energy excitations with the off-diagonal blocks included. The data are extremely similar to those of column 3, with very small differences in the order of 0.01 eV. For most practical purposes, $K^{A,B}$ and $K^{B,A}$ can indeed be ignored. Albrecht *et al.*[13] have found that the absorption spectrum of bulk Si is also insensitive to the off-diagonal blocks. This gives us confidence that, at least for weakly correlated systems like Si or other semiconductors, accurate excitation energies and optical spectra can be obtained within the block-diagonal approximation. It is important to note, however, that this behavior may not be true for other methods. In other methods like, e.g., TDDFT, the interaction kernel $K^{e,h}$ may describe a different type of interaction Hamiltonian and its off-diagonal blocks may play an important role.[27]

D. Semiconductor clusters

Starting from the SiH_4 molecule discussed in the last section, we have investigated the behavior of optical excitations of semiconductor clusters of increasing size.[11] We present results for clusters ranging from SiH_4 to $Si_{14}H_{20}$, with diam-
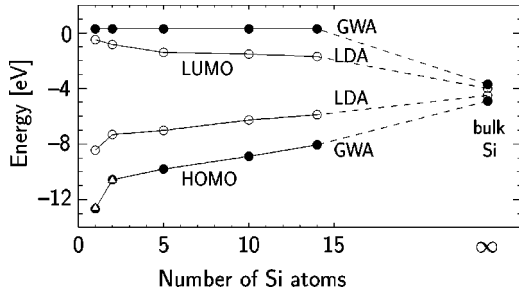
FIG. 2. HOMO and LUMO energies of Si_mH_n clusters ($m = 1$ to 14), calculated as LDA Kohn-Sham eigenvalues (○) and within GWA (●). The triangles (△) denote ionization energies measured by Itoh et al. (Ref. 30).

eters from 3 Å to 9 Å. The clusters we study in this paper can be regarded as the molecular limit of semiconductor nanostructures that have recently attracted much attention.[31] The analysis of many-body effects in the systems studied here, together with respective data on periodic crystals, allows for a more detailed understanding of electronic correlation in the entire range of semiconductor systems from the molecular to the nanoscale and macroscopic regime.

Figure 2 shows the LDA and *GW* QP energies of the HOMO state of each cluster. The size dependence of the LDA energies is mostly given by the quantum confinement effect. In the limit of infinitely large clusters, the LDA HOMO energy should reach the LDA valence-band maximum (VBM) of H-terminated Si surfaces, for which we obtain −4.5 eV with respect to the vacuum level. The QP corrections of the HOMO of our clusters (ranging from 4.2 eV to 2.2 eV) are much larger than the QP correction of 0.4 eV of the VBM of bulk Si. This results from the much weaker dielectric screening of the clusters as compared to bulk Si. In the limit of infinitely large clusters, the QP correction of the HOMO should be 0.4 eV and its QP energy should amount to −4.9 eV. For all clusters shown here, the LUMO state is bound in LDA but unbound in GWA (see the discussion above). For $N \rightarrow \infty$, the LUMO should reach the bulk values of −4.0 eV in LDA and −3.7 eV in GWA.

Figure 3 shows the excitation energies of the lowest spin-triplet, spin-singlet, and dipole-allowed spin-singlet excitations. All three transition energies exhibit the expected quantum-confinement behavior, i.e., they decrease as the number of Si atoms in the clusters increases. For infinitely large systems, the lowest-energy spin-singlet and -triplet states should converge towards the fundamental bulk band
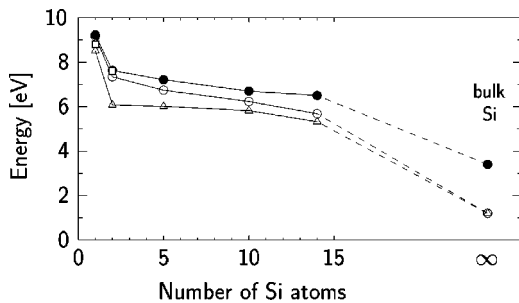

FIG. 3. Excitation energies of the lowest spin-triplet (△ up), spin-singlet (○), and dipole-allowed spin-singlet (●) excitations of the Si_mH_n clusters. The experimental data (□) are from Ref. 30.

gap of Si (1.17 eV), corrected for the excitonic binding energy of 0.015 eV. The singlet-triplet splitting, which is on the order of 1 eV for the small clusters, nearly vanishes in extended systems. The lowest dipole-allowed spin-singlet transition that is relevant for the onset of the optical spectrum, should not converge towards the fundamental bulk band gap of Si, but towards the minimum direct band gap, corrected for excitonic effects, which is at about 3.4 eV (see Sec. IV B). Figure 3 shows that the difference between the lowest-energy spin-singlet transition and the first significantly dipole-allowed transition increases with increasing cluster size. The optical absorption spectra of SiH_4 and of Si_2H_6 have been measured by Itoh et al.[30] The lowest-energy dipole-allowed transition energies are 8.8 eV and 7.6 eV, respectively (included in Fig. 3). Our calculated results of 9.2 eV and 7.6 eV are in good agreement with these data.

IV. PERIODIC CRYSTALS: SEMICONDUCTORS AND INSULATORS

In the previous section, the extreme case of small, three-dimensionally confined systems was examined. In this section we investigate the other extreme case of condensed-matter materials, i.e., infinitely extended periodic crystals. As illustrations we discuss the optical spectra of the semiconductors GaAs and Si, as well as those of the insulators LiF and LiCl. Before we turn to these results, however, some technical issues related to the periodicity of the crystals have to be addressed.

A. Technical details

In periodic systems, such as crystals, crystal surfaces, and polymer chains, some further specifications of the formalism presented in Sec. II C are necessary. The single-particle states are now given as $|\psi_{nk}\rangle$ with the wave vector **k** in the first Brillouin zone. The two-particle excitations of Eq. (16) are now given as

$$|N,S\rangle = \sum_{\mathbf{k}} \sum_{v}^{hole} \sum_{c}^{elec} A_{vck}^S \hat{a}_{vk}^\dagger \hat{b}_{c,\mathbf{k}+\mathbf{Q}}^\dagger |N,0\rangle$$

$$=: \sum_{\mathbf{k}} \sum_{v}^{hole} \sum_{c}^{elec} A_{vc}^S |vc\mathbf{k}\rangle, \qquad (33)$$

where **Q** is the total momentum of the two-particle state. In analogy to Bloch's theorem for the single-particle problem, **Q** is a well-defined quantum number for the two-particle states, and the excitations can be classified with respect to **Q**. In an optical excitation process, **Q** is the momentum of the photon that is absorbed by the two-particle state. The magnitude of the photon momentum is usually very small and is thus unimportant in the present context. Its direction, on the other hand, is significant for the nonanalytical long-range exchange term of the electron-hole interaction. In the case of the degenerate valence bands in cubic crystals, e.g., it leads to the splitting of the excitons into transverse and longitudinal modes. Nonzero **Q** vectors are relevant for bound exciton states in materials with an indirect fundamental gap.

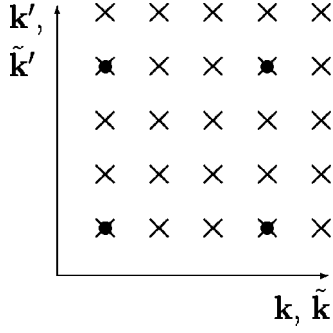The electron-hole interaction matrix elements are now given by

FIG. 4. Illustration of the interpolation scheme of the electron-hole interaction in reciprocal space. The dots ($\bullet$) denote combinations of wave vectors $(\widetilde{\mathbf{k}},\widetilde{\mathbf{k}}')$ for which the interaction matrix elements are *calculated*. The crosses ($\times$) denote combinations of wave vectors $(\mathbf{k},\mathbf{k}')$ for which the matrix elements are obtained by the interpolation scheme of Eq. (47). Thereafter, the BSE is solved on the grid $\{\times\}$. Note that each of the two axes represents a three-dimensional reciprocal space.

$$\langle vc\mathbf{k}|K^{eh,d}|v'c'\mathbf{k}'\rangle = -\int d\mathbf{x}\,d\mathbf{x}'\,\psi^*_{c,\mathbf{k}+\mathbf{Q}}(\mathbf{x})\psi_{c',\mathbf{k}'+\mathbf{Q}}(\mathbf{x})$$
$$\times W(\mathbf{r},\mathbf{r}')\psi_{v\mathbf{k}}(\mathbf{x}')\psi^*_{v'\mathbf{k}'}(\mathbf{x}') \quad (34)$$

(neglecting the frequency dependence of W) and

$$\langle vc\mathbf{k}|K^{eh,x}|v'c'\mathbf{k}'\rangle = \int d\mathbf{x}\,d\mathbf{x}'\,\psi^*_{c,\mathbf{k}+\mathbf{Q}}(\mathbf{x})\psi_{v\mathbf{k}}(\mathbf{x})v(\mathbf{r},\mathbf{r}')$$
$$\times \psi_{c',\mathbf{k}'+\mathbf{Q}}(\mathbf{x}')\psi^*_{v'\mathbf{k}'}(\mathbf{x}'). \quad (35)$$

In semiconductor crystals, several occupied and unoccupied bands v and c, as well as several hundred wave vectors $\mathbf{k}$, i.e., up to 10^4 basis functions, are necessary to represent the transitions $|S\rangle$ relevant to the optical spectrum. The determination of the $\sim 10^8$ matrix elements of the electron-hole interaction, each of which requires a multidimensional integration given by Eqs. (34) and (35), forms a major bottleneck. In order to make the calculations feasible, we have developed a novel interpolation scheme with respect to reciprocal-space vectors (see Fig. 4). The main idea is to calculate the interaction only for some points $(\widetilde{\mathbf{k}},\widetilde{\mathbf{k}}')$ on a coarse grid in reciprocal space [indicated as ($\bullet$) in Fig. 4], and then to interpolate onto a much finer grid $\{(\mathbf{k},\mathbf{k}')\}$ required for the BSE [indicated as ($\times$)]. In this interpolation, particular attention has to be paid to the divergent behavior of the Coulomb interaction in the limit $\mathbf{k}\rightarrow\mathbf{k}'$ and to the phases of the wave functions (see below).

The general idea of the interpolation scheme is the following. Let $f(\mathbf{r},\mathbf{r}')$ be a lattice-periodic two-point function (later, this will be the bare and screened Coulomb interaction). f can be written in terms of its Fourier transform,

$$f(\mathbf{r},\mathbf{r}') = \sum_{\mathbf{q}\mathbf{G}\mathbf{G}'} e^{-i(\mathbf{q}+\mathbf{G})\cdot\mathbf{r}}f_{\mathbf{G},\mathbf{G}'}(\mathbf{q})e^{i(\mathbf{q}+\mathbf{G}')\cdot\mathbf{r}'}$$
$$=: \sum_{\mathbf{q}} e^{-i\mathbf{q}\cdot\mathbf{r}}f_{\mathbf{q}}(\mathbf{r},\mathbf{r}')e^{i\mathbf{q}\cdot\mathbf{r}'}. \quad (36)$$

$f_{\mathbf{q}}(\mathbf{r},\mathbf{r}')$ is a double-periodic function, i.e., it is lattice-periodic in both $\mathbf{r}$ and $\mathbf{r}'$ separately. Using Eq. (36), a six-dimensional integral of f in the structure of, e.g., Eq. (34), is calculated as

$$\langle vc\widetilde{\mathbf{k}}|f|v'c'\widetilde{\mathbf{k}}'\rangle$$
$$\equiv \int d\mathbf{x}\,d\mathbf{x}'\,\psi^*_{c\widetilde{\mathbf{k}}}(\mathbf{x})\psi_{c'\widetilde{\mathbf{k}}'}(\mathbf{x})f(\mathbf{r},\mathbf{r}')\psi_{v\widetilde{\mathbf{k}}}(\mathbf{x}')\psi^*_{v'\widetilde{\mathbf{k}}'}(\mathbf{x}')$$
$$= \int d\mathbf{x}\,d\mathbf{x}'\,u^*_{c\widetilde{\mathbf{k}}}(\mathbf{x})u_{c'\widetilde{\mathbf{k}}'}(\mathbf{x})f_{\widetilde{\mathbf{q}}}(\mathbf{r},\mathbf{r}')u_{v\widetilde{\mathbf{k}}}(\mathbf{x}')u^*_{v'\widetilde{\mathbf{k}}'}(\mathbf{x}')$$
$$=: \langle vc\widetilde{\mathbf{k}}|f_{\widetilde{\mathbf{q}}}|v'c'\widetilde{\mathbf{k}}'\rangle \quad (37)$$

where $u_{n\widetilde{\mathbf{k}}}(\mathbf{x}) = e^{-i\widetilde{\mathbf{k}}\cdot\mathbf{r}}\psi_{n\widetilde{\mathbf{k}}}(\mathbf{x})$ is the lattice-periodic part of the wave function n at wave vector $\widetilde{\mathbf{k}}$. Of the sum over $\mathbf{q}$ in Eq. (36), only $\widetilde{\mathbf{q}} = (\widetilde{\mathbf{k}}'-\widetilde{\mathbf{k}})$ contributes to Eq. (37).

After calculating such matrix elements on the coarse grid $\{\widetilde{\mathbf{k}},\widetilde{\mathbf{k}}'\}$ (indicated schematically as ($\bullet$) in Fig. 4), the main problem remains in evaluating the corresponding matrix elements for a pair of wave vectors $(\mathbf{k},\mathbf{k}')$ different from $(\widetilde{\mathbf{k}},\widetilde{\mathbf{k}}')$. This requires an appropriate interpolation scheme in the six-dimensional reciprocal space, which can be done as follows.

For any given wave vector $\widetilde{\mathbf{k}}$, the lattice-periodic functions $u_{n\widetilde{\mathbf{k}}}(\mathbf{x})$ form a complete set in which any other lattice-periodic function can be expanded. This holds in particular for the lattice-periodic part u of a wave function n at another wave vector $\mathbf{k}$:

$$u_{n\mathbf{k}}(\mathbf{x}) = \sum_{\widetilde{n}} d_{n\mathbf{k}}^{\widetilde{n}\widetilde{\mathbf{k}}}u_{\widetilde{n}\widetilde{\mathbf{k}}}(\mathbf{x}). \quad (38)$$

By applying the operation $\int d\mathbf{x}\,u^*_{m\widetilde{\mathbf{k}}}(\mathbf{x})$ to Eq. (38) and using the orthonormality of the wave functions at $\widetilde{\mathbf{k}}$, one obtains that the coefficients $d_{n\mathbf{k}}^{\widetilde{n}\widetilde{\mathbf{k}}}$ are given as

$$d_{n\mathbf{k}}^{\widetilde{n}\widetilde{\mathbf{k}}} = \int d\mathbf{x}\,u^*_{n\widetilde{\mathbf{k}}}(\mathbf{x})u_{n\mathbf{k}}(\mathbf{x}). \quad (39)$$

By employing Eq. (38), a matrix element $\langle vc\mathbf{k}|f|v'c'\mathbf{k}'\rangle$ of Eq. (37) can be obtained as

$$\langle vc\mathbf{k}|f|v'c'\mathbf{k}'\rangle$$
$$= \sum_{\widetilde{n}_1\widetilde{n}_2\widetilde{n}_3\widetilde{n}_4} d_{v\mathbf{k}}^{\widetilde{n}_1\widetilde{\mathbf{k}}}(d_{c\mathbf{k}}^{\widetilde{n}_2\widetilde{\mathbf{k}}})^*(d_{v'\mathbf{k}'}^{\widetilde{n}_3\widetilde{\mathbf{k}}'})^*d_{c'\mathbf{k}'}^{\widetilde{n}_4\widetilde{\mathbf{k}}'}\langle\widetilde{n}_1\widetilde{n}_2\widetilde{\mathbf{k}}|f_{\mathbf{q}}|\widetilde{n}_3\widetilde{n}_4\widetilde{\mathbf{k}}'\rangle$$
$$\approx \sum_{\widetilde{n}_1\widetilde{n}_2\widetilde{n}_3\widetilde{n}_4} d_{v\mathbf{k}}^{\widetilde{n}_1\widetilde{\mathbf{k}}}(d_{c\mathbf{k}}^{\widetilde{n}_2\widetilde{\mathbf{k}}})^*(d_{v'\mathbf{k}'}^{\widetilde{n}_3\widetilde{\mathbf{k}}'})^*d_{c'\mathbf{k}'}^{\widetilde{n}_4\widetilde{\mathbf{k}}'}\langle\widetilde{n}_1\widetilde{n}_2\widetilde{\mathbf{k}}|f_{\widetilde{\mathbf{q}}}|\widetilde{n}_3\widetilde{n}_4\widetilde{\mathbf{k}}'\rangle.$$
$$(40)$$

The step from the first to the second line in Eq. (40) is an approximation since $\mathbf{q} = (\mathbf{k}'-\mathbf{k})$ is replaced by $\widetilde{\mathbf{q}} = (\widetilde{\mathbf{k}}'-\widetilde{\mathbf{k}})$. Several issues must be discussed in the context of Eq. (40). The transformation is only exact if the four summations run over all indices $(1,\ldots,\infty)$ and if $\mathbf{q} = \widetilde{\mathbf{q}}$ (or if $f_{\mathbf{q}} = f_{\widetilde{\mathbf{q}}}$). For practical purposes, however, the summations must be truncated to a very small subset of states, and the set of $\widetilde{\mathbf{q}}$ vectors

can only be finite, so $f_{\mathbf{q}}=f_{\tilde{\mathbf{q}}}$ is usually not exactly valid. For $f_{\mathbf{q}}$ being the (screened or bare) Coulomb interaction, this poses a severe problem. This can best be demonstrated by expanding the screened Coulomb interaction in terms of its Fourier transform:

$$W(\mathbf{r},\mathbf{r}') = \sum_{\mathbf{q}\mathbf{G}\mathbf{G}'} e^{-i(\mathbf{q}+\mathbf{G})\cdot\mathbf{r}} \frac{\epsilon_{\mathbf{G},\mathbf{G}'}^{-1}(\mathbf{q})}{|\mathbf{q}+\mathbf{G}||\mathbf{q}+\mathbf{G}'|} e^{i(\mathbf{q}+\mathbf{G}')\cdot\mathbf{r}'}. \tag{41}$$

Some terms in Eq. (41), i.e., the ones with $\mathbf{G}=\mathbf{0}$ and/or $\mathbf{G}'=\mathbf{0}$, behave as $1/q^2$ and $1/q$. Therefore the matrix elements of K^d depend very sensitively on the reciprocal distance $\mathbf{q}$, in particular when q is small, i.e., the condition $f_{\mathbf{q}}\approx f_{\tilde{\mathbf{q}}}$ is not fulfilled. An interpolation scheme directly for K^d would thus be very unstable and converge extremely slowly with respect to the density of the grid $\{\tilde{\mathbf{q}}\}$.

Instead, we decompose K^d into three contributions, motivated by the Fourier series for W. Corresponding to Eq. (41), the matrix elements of K^d are given as double summations over $\mathbf{G}$ and $\mathbf{G}'$. For small $\mathbf{q}$, the "head" ($\mathbf{G}=\mathbf{G}'=\mathbf{0}$) and the "wings" ($\mathbf{G}=\mathbf{0}$ or $\mathbf{G}'=\mathbf{0}$) of W behave as $1/q^2$ and $1/q$, respectively, whereas all other matrix elements of W remain finite. Concomitantly the matrix elements of K^d can be written as

$$\langle vc\mathbf{k}|K^{eh,d}|v'c'\mathbf{k}'\rangle = \frac{a_{vc\mathbf{k},v'c'\mathbf{k}'}}{q^2} + \frac{b_{vc\mathbf{k},v'c'\mathbf{k}'}}{q} + c_{vc\mathbf{k},v'c'\mathbf{k}'}, \tag{42}$$

with

$$a_{vc\mathbf{k},v'c'\mathbf{k}'} = M_{cc'}^{\mathbf{0}}(\mathbf{k}+\mathbf{Q},\mathbf{q})\epsilon_{\mathbf{0},\mathbf{0}}^{-1}(\mathbf{q})[M_{vv'}^{\mathbf{0}}(\mathbf{k},\mathbf{q})]^*, \tag{43}$$

$$b_{vc\mathbf{k},v'c'\mathbf{k}'} = \sum_{\mathbf{G}} \left\{ M_{cc'}^{\mathbf{G}}(\mathbf{k}+\mathbf{Q},\mathbf{q})\frac{\epsilon_{\mathbf{G},\mathbf{0}}^{-1}(\mathbf{q})}{|\mathbf{q}+\mathbf{G}|}[M_{vv'}^{\mathbf{0}}(\mathbf{k},\mathbf{q})]^* \right.$$
$$\left. + M_{cc'}^{\mathbf{0}}(\mathbf{k}+\mathbf{Q},\mathbf{q})\frac{\epsilon_{\mathbf{0},\mathbf{G}}^{-1}(\mathbf{q})}{|\mathbf{q}+\mathbf{G}|}[M_{vv'}^{\mathbf{G}}(\mathbf{k},\mathbf{q})]^* \right\}, \tag{44}$$

$$c_{vc\mathbf{k},v'c'\mathbf{k}'} = \sum_{\mathbf{G}\neq\mathbf{0}} \sum_{\mathbf{G}'\neq\mathbf{0}} M_{cc'}^{\mathbf{G}}(\mathbf{k}+\mathbf{Q},\mathbf{q})\frac{\epsilon_{\mathbf{G},\mathbf{0}}^{-1}(\mathbf{q})}{|\mathbf{q}+\mathbf{G}||\mathbf{q}+\mathbf{G}'|}$$
$$\times [M_{vv'}^{\mathbf{G}'}(\mathbf{k},\mathbf{q})]^*. \tag{45}$$

The matrix elements $M_{mn}^{\mathbf{G}}(\mathbf{k},\mathbf{q})$ are calculated as

$$M_{mn}^{\mathbf{G}}(\mathbf{k},\mathbf{q}) = \int d\mathbf{x}\, \psi_{m,\mathbf{k}}^*(\mathbf{x}) e^{-i(\mathbf{q}+\mathbf{G})\cdot\mathbf{r}}\psi_{n,\mathbf{k}+\mathbf{q}}(\mathbf{x}). \tag{46}$$

The coefficients a, b, and c fulfill the requirement that their underlying integration kernels are doubly lattice-periodic (see above). They can thus be calculated employing the interpolation scheme of Eq. (40). In particular, a, b, and c vary only weakly with respect to $\mathbf{k}$ and $\mathbf{k}'$. Furthermore, the wave functions $u_{n\mathbf{k}}$ also vary only fairly weakly with respect to $\mathbf{k}$ (apart from sudden band crossing; see below). To be more precise, a state $u_{n\mathbf{k}}$ at $\mathbf{k}$ can be expressed with high accuracy with only a few states $\tilde{n}$ at $\tilde{\mathbf{k}}$. Therefore, the

band summation of Eq. (40) can be restricted to very few bands without losing significant accuracy. In the actual calculations, we restrict n_1 and n_3 to the same set of valence bands and n_2 and n_4 to the same set of conduction bands that are finally included in the BSE:

$$a_{vc\mathbf{k},v'c'\mathbf{k}'} = \sum_{\tilde{v}\tilde{c}\tilde{v}'\tilde{c}'} d_{v\mathbf{k}}^{\tilde{v}\tilde{\mathbf{k}}}(d_{c\mathbf{k}}^{\tilde{c}\tilde{\mathbf{k}}})^*(d_{v'\mathbf{k}'}^{\tilde{v}'\tilde{\mathbf{k}}'})^* d_{c'\mathbf{k}'}^{\tilde{c}'\tilde{\mathbf{k}}'} a_{\tilde{v}\tilde{c}\tilde{\mathbf{k}},\tilde{v}'\tilde{c}'\tilde{\mathbf{k}}'} \tag{47}$$

and the same expression for the coefficients b and c.

The exchange interaction matrix elements K^x of Eq. (35) do not suffer from the divergent behavior of the Coulomb interaction. Since the occupied (v) and empty (c) states are orthogonal, the integrals $M_{vc}^{\mathbf{0}}(\mathbf{k},\mathbf{q})$ in Eq. (35) are proportional to q for $q\rightarrow 0$, thus leading to a finite value of the interaction matrix elements. Therefore our interpolation scheme applies directly to K^x, and a decomposition into some coefficients (as for K^d) is not necessary.

The decomposition of K^d into the coefficients a, b, and c was motivated by the corresponding plane-wave representation of the screened Coulomb interaction [Eq. (41)], consisting of head, wings, and body. In our Gaussian-orbital basis set, on the other hand, the structure of W is more complex. A decomposition analogous to the one described above is, nonetheless, possible and leads to the same decomposition of $K^{eh,d}$ into the three contributions a, b, and c as denoted in Eq. (42).

A very important issue is that the transformation Eq. (40) automatically takes care of the phases of the wave functions $\psi_{n\mathbf{k}}$. From Eq. (28) it becomes obvious that the phases are crucial to describe constructive and destructive coherence correctly. To be more precise, the phases of the wave functions (which are totally arbitrary) must be treated consistently in the optical oscillator strength *and* in the electron-hole interaction matrix elements. Since a numerical diagonalization procedure of the single-particle Hamiltonian will yield random phases for the single-particle wave functions, the evaluation of Eq. (47) is a definitive way of treating the phases in a controlled way when constructing the interaction matrix elements by interpolation. Otherwise the phase information will not be transferred to the optical transition matrix elements correctly and the optical spectrum will be more or less given by the random-phase approximation (apart from some minor energy shifts due to the attractive nature of the interaction). To faciliate the computations, it is helpful to define the phases of the single-particle wave functions in a unique way that is kept throughout the calculations. One possibility is to require that the sum of the basis-set coefficients of the wave function be real.

A concrete example of the interpolation scheme is presented in Fig. 5. The figure shows the real part of a matrix element ($v=v'=4=$highest valence band, $c=c'=5$ =lowest conduction band) of the direct term of the electron-hole interaction of GaAs (multiplied by q^2 for sake of clarity). The vectors $\mathbf{k}$, $\mathbf{k}'$, $\tilde{\mathbf{k}}$, and $\tilde{\mathbf{k}}'$, and $\mathbf{q}$ are indicated in panel (a). The wave vectors $\mathbf{k}$ and $\mathbf{k}'$ start at A and run along two different directions, [100] and [010]. The difference vector q increases from 0 to $0.7(2\pi/a)$. Panel (b) shows three results of the matrix element, based on three starting points of the interpolation scheme [$(\tilde{\mathbf{k}},\tilde{\mathbf{k}}')=$(A,A'),(B,B'), and
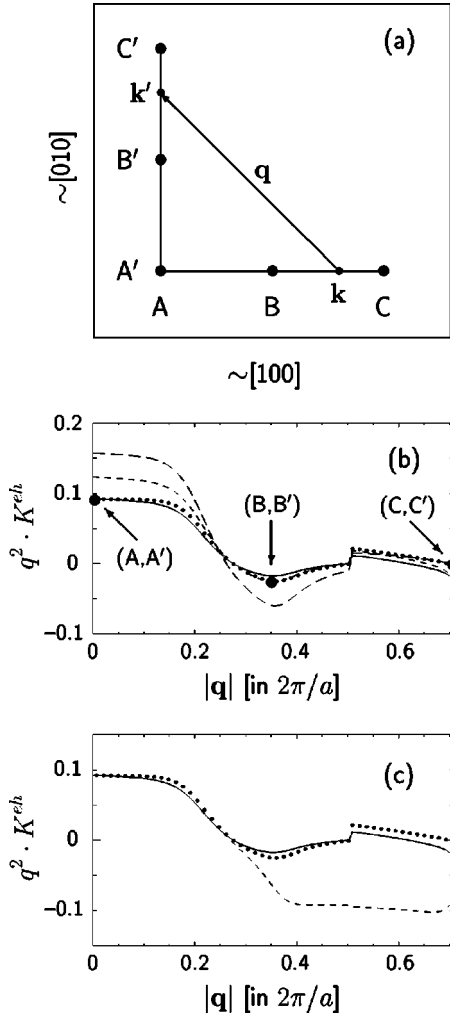
FIG. 5. Illustration of the interpolation scheme of the electron-hole interaction, for the example of the matrix element $\langle 45\mathbf{k}|K^{eh,d}|45\mathbf{k}'\rangle$ (real part only) between the highest valence band ($=4$) and the lowest conduction band ($=5$) of bulk GaAs. (a) Geometric arrangement of the points and vectors $\mathbf{k}$, $\mathbf{k}'$, $\widetilde{\mathbf{k}}$, and $\widetilde{\mathbf{k}}'$ in the Brillouin zone. All points are in a (001) plane, in units of $2\pi/a$. The capital letters denote the points $A=A'=(-3/4,-1/4,-1/4)$, $B=(-1/2,-1/4,-1/4)$, $C=(-1/4,-1/4,-1/4)$, $B'=(-3/4,0,-1/4)$, and $C'=(-3/4,1/4,-1/4)$. (b) Real part of the coefficient $a_{45\mathbf{k},45\mathbf{k}'}$, plotted against $|\mathbf{q}|$ with $\mathbf{q}=(\mathbf{k}'-\mathbf{k})$. $\mathbf{k}$ runs from A to C while $\mathbf{k}'$ runs from A' to C'. The three curves (——, - - - -, and — — —) denote three interpolations for $a_{45\mathbf{k},45\mathbf{k}'}$, that are based on the starting points $(\widetilde{\mathbf{k}}=A,\widetilde{\mathbf{k}}'=A')$, $(\widetilde{\mathbf{k}}=B,\widetilde{\mathbf{k}}'=B')$, and $(\widetilde{\mathbf{k}}=C,\widetilde{\mathbf{k}}'=C')$, respectively. The summations in Eq. (47) are carried out with four valence bands and six conduction bands. The dotted curve denotes the exact result. (c) Same as panel (b), but with different summations in Eq. (47). The solid curve is the same as in (b). The dashed curve is calculated with the highest valence band ($=4$) and the lowest conduction band ($=5$) only. Both interpolations are based on the starting points $(\widetilde{\mathbf{k}}=A,\widetilde{\mathbf{k}}'=A')$.

(C,C')]. The dots indicate the exact result. The solid curve shows the interpolation based on $(\widetilde{\mathbf{k}},\widetilde{\mathbf{k}}')=(A,A')$. For $q=0$ (i.e., $\mathbf{k}=\widetilde{\mathbf{k}}=A$ and $\mathbf{k}'=\widetilde{\mathbf{k}}'=A'$), it is by construction identical to the exact result, which is given by $1/\epsilon_\infty=0.092$. At the other points this interpolation agrees nicely with the exact data, but shows some deviations at larger q. The short-

dashed curve is constructed from the starting point $(\widetilde{\mathbf{k}},\widetilde{\mathbf{k}}')=(B,B')$. At this point, it coincides with the exact data, while there are significant deviations at wave vectors farther away from (B,B'). The long-dashed curve is based on the interaction matrix elements calculated at $(\widetilde{\mathbf{k}},\widetilde{\mathbf{k}}')=(C,C')$. Also for this curve, deviations appear farther away from its starting point. The main issue, however, is that all curves reproduce the exact result excellently in the vicinity of the respective starting point. Thus a coarse mesh of starting points finally leads to correct values for the electron-hole interaction in the entire reciprocal space.

An interesting and important feature is that all three interpolation curves correctly describe the "step" in the interaction at $q\approx0.5(2\pi/a)$, which results from a band crossing of the two highest valence bands of GaAs. At this point, the highest valence state rapidly changes its character and wave function. In the interpolation scheme, this effect is only reproduced because the summation in Eq. (47) includes information about the valence states other than $v=v'=4$. The importance of this summation is demonstrated explicitly in panel (c). The solid curve in this panel, which is the same as in panel (b), is calculated by including all four valence bands and the six lowest conduction bands in the summation of Eq. (47). For the dashed curve, on the other hand, only the term $(\widetilde{v}=v,\widetilde{v}'=v',\widetilde{c}=c,\widetilde{c}'=c')$ is kept, i.e., the mixing of the wave functions is fully ignored. Panel (c) shows that this unrealistic interpolation, which assumes that the wave function $u_{n\mathbf{k}}(\mathbf{x})$ of a given band n is the same for all wave vectors $\mathbf{k}$, can be well justified in the vicinity of the starting points, but can lead to totally wrong results for the electron-hole interaction for wave vectors farther away.

For periodic crystals, the BSE is an eigenvalue problem of infinite dimensionality,

$$(E^{QP}_{c,\mathbf{k}+\mathbf{Q}}-E^{QP}_{v\mathbf{k}})A^S_{vc\mathbf{k}}$$

$$+\int_{V_{BZ}}d^3k'\sum_{v',c'}\langle vc\mathbf{k}|K^{eh}|v'c'\mathbf{k}'\rangle A^S_{v'c'\mathbf{k}'}=\Omega_S A^S_{vc\mathbf{k}}.$$

$$(48)$$

The integration $\int d^3k'$ ranges over the first Brillouin zone. For a numerical evaluation, the continuous integration with respect to $\mathbf{k}'$ has to be replaced by some discrete scheme of finite dimensionality. The easiest approach is to divide the Brillouin zone into an appropriate grid (uniform or nonuniform) of subvolumes V_i, represented by one point $\mathbf{k}_i$ inside, and to assume that (i) the coefficients $A^S_{vc\mathbf{k}}$ can be represented by an average value $A^S_{vc\mathbf{k}_i}$ in V_i, taken at $\mathbf{k}_i$, and that (ii) the same holds for the band-structure energy differences $(E^{QP}_{c\mathbf{k}}-E^{QP}_{v,\mathbf{k}+\mathbf{Q}})$. In the case of a grid with equal subvolumes $V_i\equiv V$ for all i, this leads to the discrete eigenvalue problem

$$(E^{QP}_{c,\mathbf{k}_i+\mathbf{Q}}-E^{QP}_{v\mathbf{k}_i})A^S_{vc\mathbf{k}_i}$$

$$+\sum_{i'}\sum_{v',c'}\frac{1}{V}\int_{V_i}d^3k\int_{V_{i'}}d^3k'\langle vc\mathbf{k}|K^{eh}|v'c'\mathbf{k}'\rangle A^S_{v'c'\mathbf{k}_i}$$

$$=\Omega_S A^S_{vc\mathbf{k}_i}.$$

$$(49)$$

The integration of the electron-hole interaction with respect to **k** and **k**′ requires special care due to the divergence for **k**→**k**′ [cf. Eq. (42)]. In particular, a careful six-dimensional integration of the kernels $1/|\mathbf{k}-\mathbf{k}'|^2$ and $1/|\mathbf{k}-\mathbf{k}'|$ over the product volume $V_i V_i'$ is required. We do this by numerical integration on different subgrids and extrapolating to zero grid spacing. In many situations, it may be desirable to use nonuniform **k** grids to sample sensitive regions of the Brillouin zone with increased accuracy, or to use different **k** grids for different band-band combinations (v,c) (for instance, if some bands are highly dispersive and others are not). Both extensions of the approach are possible but require additional considerations because the basis states $|vc\mathbf{k}_i\rangle$ will have different weights $(\sim 1/V_i)$ in the excitations $|S\rangle$. In fact, the configurations $|vc\mathbf{k}_i\rangle$ then form a basis that is still orthogonal but no longer normalized. Concomitantly, the BSE is no longer given by a standard eigenvalue problem but by a generalized eigenvalue problem instead, with an overlap matrix $S_{ii'} = \delta_{ii'} V_i$ that is still diagonal but not unity.

B. Semiconductors: GaAs and Si

The focus of this section is on the resonant optical spectrum of semiconductors above the fundamental gap energy E_g, up to a maximum energy of several E_g.[11] Similar studies were carried out by Albrecht *et al.*[13] [8] and by Benedict *et al.*[14] Bound excitons below E_g are not considered here. We have discussed the bound excitons in GaAs in Ref. 11.

The evaluation of the BSE was carried out with the three highest valence bands and the six lowest conduction bands. The electron-hole interaction was calculated for 32 wave vectors $\tilde{\mathbf{k}}$ in the first Brillouin zone, i.e., at the points $(\frac{1}{4},\frac{1}{4},\frac{1}{4})(2\pi/a)$ and $(\frac{3}{4},\frac{1}{4},\frac{1}{4})(2\pi/a)$ and the corresponding stars. Thereafter, the interpolation scheme of Eqs. (42) and (47) was employed to obtain the interaction matrix elements for 500 **k** points in the Brillouin zone. These 500 points form a cubic grid with a mesh distance of $0.2(2\pi/a)$. One important issue is that the grid is not symmetric with respect to the Brillouin zone. Instead, it is slightly shifted in a direction different from the high-symmetry directions of the crystal. This leads to a finer sampling of the spectrum of free electron-hole pairs. An unshifted grid would correspond to only 28 crystallographically different points, which are much too few to achieve a good spectral resolution. The random shift, on the other hand, leads to a grid of 500 crystallographically different wave vectors, which gives a spectral resolution of about 0.15 eV, sufficient to compare the calculated spectra with experimental data.

To check the applicability of the interpolation scheme, we have carried out calculations based on different coarse grids $\{\tilde{\mathbf{k}}\}$. It turns out that the final spectra are very stable with respect to the coarse grid. From the coarse grid of 32 $\tilde{\mathbf{k}}$ points, we obtain essentially the same spectrum of GaAs as we get from a coarse grid with 108 points. The uncertainties from using the coarse grid of only 32 points are smaller than 1% for transition energies and smaller than 5% for oscillator strengths. The evaluation of the spatial integration in Eqs. (34) and (35) is the most demanding step of the entire approach. The use of the interpolation scheme reduces this step from 500×500 evaluations to only 32×32 evaluations, i.e., by a factor of 240.
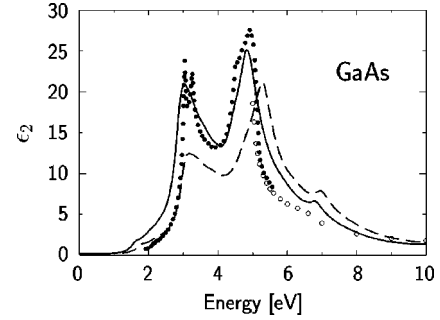

FIG. 6. Calculated optical absorption spectrum of GaAs with (solid lines) and without (dashed lines) electron-hole interaction, using three valence bands, six conduction bands, 500 **k** points in the BZ, and an artificial broadening of 0.15 eV. The dots denote experimental data from Ref. 32 (○) and Ref. 33 (●).

Figure 6 shows the optical spectrum of GaAs, calculated with (solid lines) and without (dashed lines) electron-hole interaction. The dots denote experimental data.[32,33] The spectrum resulting from the free quasiparticle interband transitions shows systematic deviations from experiment. At low energies (2–5 eV) the absorption strength is much lower than in experiment while it is too high for energies above 5 eV. When we include the electron-hole interaction, the peaks at 3 eV and at 5 eV are strongly enhanced; in addition, the peak structure at 5 eV is effectively shifted to lower energies. The spectrum including the interaction is in much better agreement with the measured data. Some fine structures of the measured data, such as the splitting of the 3 eV peak, are, however, not observed in the calculation. This splitting of 0.2 eV is due to spin-orbit splitting at high-symmetry points of the band structure. To observe these details in the calculation, the **k**-point grid must be refined to reach a spectral resolution of about 0.05 eV, and the spin variables must be included explicitly since spin-singlet and -triplet excitations are coupled by the spin-orbit interaction.

The modifications of the optical spectrum do not result from a negative shift of the transition energies, as one might naively expect from the attractive nature of the electron-hole interaction. To illustrate this point, we present in Fig. 7 the interband joint density of states and the density of excited states (divided by ω^2 to make it comparable to the absorption spectrum) for the electron-hole transitions without and with the electron-hole interaction, respectively. It is obvious that the density of excited states remains nearly unchanged by the
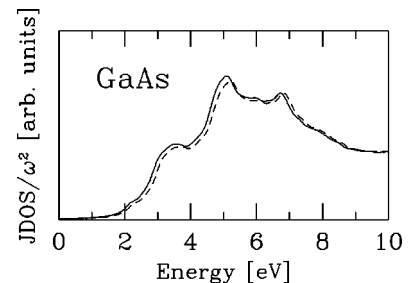

FIG. 7. Density of excited states for GaAs divided by ω^2 (in arbitrary units). The dashed line corresponds to vertical band-to-band transitions while the solid line results from the BSE, including the electron-hole interaction.
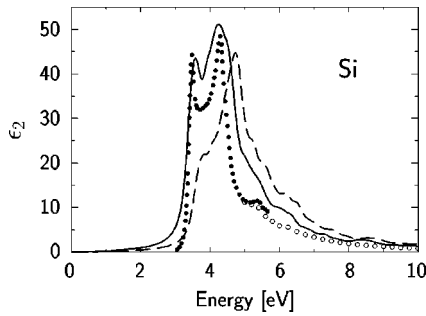
FIG. 8. Calculated optical absorption spectrum of Si with (solid lines) and without (dashed lines) electron-hole interaction, using three valence bands, six conduction bands, 500 **k** points in the BZ, and an artificial broadening of 0.15 eV. Experimental data are taken from Ref. 34 (○) and Ref. 35 (●).
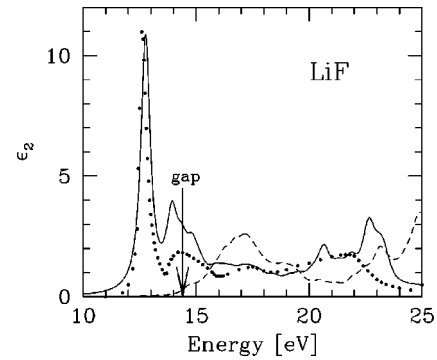

FIG. 9. Calculated optical absorption spectrum of LiF with (solid lines) and without (dashed lines) electron-hole interaction, using three valence bands, six conduction bands, 500 **k** points in the BZ, and an artificial broadening of 0.25 eV. The experimental data (●) are from Ref. 36.

interaction (with the exception of bound excitonic states below E_g, which are not visible in the present calculation). The changes in the optical spectrum originate from a completely different effect: they are due to the coherent coupling of the optical transition matrix elements in the excited-state wave function [cf. Eq. (28)], which leads to a constructive superposition of the oscillator strengths for transitions at lower energies and to a destructive superposition at energies above 5 eV. Concerning the optical spectra above E_g, this coherent coupling is much more important than the energetic shift of the excitations. Such modifications of the spectrum also occur in other semiconductors.[10,11,13,14] We have found similar behavior in low-dimensional systems like polymers and surfaces.[11]

In Fig. 8 the optical absorption spectrum of Si is presented. Again, the solid (dashed) curve shows the spectrum with (without) the electron-hole interaction, respectively. The dots denote measured data.[34,35] The effects of the interaction on the spectrum are basically the same as in the case of GaAs. Again, the final spectrum is in much better agreement with the experimental data than the independent-particle spectrum. This holds in particular for the sharp peak at 3.4 eV. The nature of this peak in the experimental spectrum has been under discussion for a long time. Our results clearly show from *ab initio* that the peak originates from excitonic effects.

Bound excitons that occur in the low-energy onset of the optical spectrum of semiconductors are not discussed here. They are not seen in Figs. 6 and 8, neither in the measured nor in the calculated spectra. In the measured data, the excitons are not observed due to the limited resolution in the data shown here. Since the binding energy of excitons amounts to only a few meV in semiconductors, a much higher spectral resolution is required. In the calculation, the spectral resolution is also not sufficient to show the excitons. This is related to the density of the **k**-point grid used. In Eq. (33), the bound excitons are composed from **k** points in the very vicinity of the minimum gap (which is at the Γ point in the case of GaAs). This region of the Brillouin zone must be sampled with a very high density to represent the excitons. Our method together with such a high-density mesh, which can be restricted to the vicinity of the minimum gap, does give correctly the bound excitons in great detail (see the discussion on GaAs in Ref. 11).

C. Insulators: LiF and LiCl

In wide-band-gap insulators the dielectric screening is much weaker than that in semiconductors. The dielectric constants of LiF and LiCl, for instance, are only 1.9 and 2.6, respectively, compared to 10.9 and 11.7 in GaAs and Si. Concomitantly the electron-hole interaction is much stronger and its effects on the optical spectra are much more pronounced.[11] As an example, Fig. 9 shows the absorption spectrum of LiF.

Over the entire energy range, the spectrum is completely altered from the noninteracting case. Again the spectrum including the interaction is in much better agreement with experiment, as was also found by Benedict *et al.*[14] The most striking feature in the calculated spectrum is the occurrence of two strongly bound singlet excitons at 12.8 eV (transverse excitons). In addition, a longitudinal singlet exciton, which is not visible in the optical spectrum, is found at 13.3 eV.

The occurrence of excitons is much more pronounced in insulators than in semiconductors. In the case of GaAs, e.g., excitonic binding takes place on a meV energy scale and the formation of the exciton only includes states very close to the Γ point of the Brillouin zone (see above). In insulators, on the other hand, the much lower dielectric constant and the usually larger effective masses of the less dispersive bands lead to excitonic coupling over the entire Brillouin zone and increase the binding energy to as much as 1.5 eV in LiF.

The strong modification of the spectra of insulators by excitonic effects makes it difficult to obtain reliable band-structure data from the measured spectra. Fundamental gap energies, for instance, can only be estimated by assuming specific values for excitonic binding energies. Our present approach allows us to apply a reverse procedure by calculating the QP band structure and the optical spectrum from first principles. The comparison of the optical spectrum with experimental data may be used to deduce whether the underlying calculated band structure is correct or not. In the present case of LiF, the calculated band gap is 14.4 eV and the calculated exciton is at 12.8 eV. The *measured* exciton energy is at 12.7 eV, i.e., it is 0.1 eV lower than the calculated one. We thus conclude that the true fundamental band gap of LiF is near 14.3 eV.

Based on the calculated imaginary part $\epsilon_2(\omega)$ of the dielectric function, the real part is obtained by a Kramers-
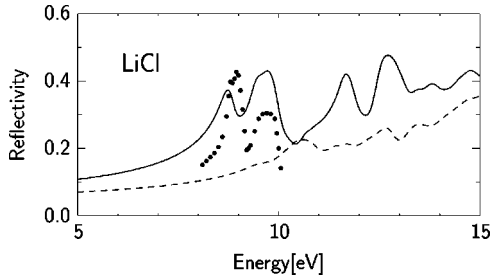
FIG. 10. Calculated reflectivity spectrum of LiCl with (solid lines) and without (dashed lines) electron-hole interaction, using three valence bands, six conduction bands, 500 **k** points in the BZ, and an artificial broadening of 0.25 eV. The experimental data (●) are from Ref. 37.

Kronig transformation, and all optical constants can be evaluated. This often allows for a more direct comparison between theory and experiment. Optical experiments (like reflectivity measurements) are sometimes limited to a certain energy range, which may not be wide enough to carry out a careful Kramers-Kronig analysis. In such cases, it would be more appropriate to directly compare the measured *reflectivity* spectrum with the calculated one. As an example, we show in Fig. 10 the reflectivity spectrum of LiCl. As in the other figures, the solid (dashed) curve shows the spectrum calculated with (without) the electron-hole interaction, respectively. The QP band structure has a fundamental gap of 9.2 eV.

The independent-particle spectrum does not have much structure. By the interaction, the reflectivity is enhanced at all energies and shows a number of sharp peaks. In particular, two peaks arise close to the gap energy, i.e., one exciton peak at 8.7 eV (below E_g) and a broader structure at 9.5–9.7 eV (above E_g). At 9.0 eV, i.e., 0.2 eV below E_g, the calculated reflectivity has a minimum. These features correspond well to the respective structures in the measured spectrum: one peak at 8.9 eV, a broader structure at 9.6–9.8 eV, and a minimum at 9.3 eV. Since there is a shift of 0.2 eV between the measured and calculated features, we conclude that the real fundamental gap energy of LiCl is likely to be at 0.2 eV higher energy than our calculated value, i.e., it is near 9.4 eV in reality.

D. Two-particle wave function

Our approach allows to explicitly calculate the wave function of an electron-hole excitation $|S\rangle$ in real space. The wave function is given by Eq. (11) with the coefficients B_{vc}^S set to zero. For a periodic system, this yields

$$\chi_S(\mathbf{x}_e, \mathbf{x}_h) = \sum_{\mathbf{k}} \overset{\text{hole}}{\sum_{v}} \overset{\text{elec}}{\sum_{c}} A_{vc\mathbf{k}}^S \psi_{c,\mathbf{k}+\mathbf{Q}}(\mathbf{x}_e) \psi_{v\mathbf{k}}^*(\mathbf{x}_h). \quad (50)$$

The wave function is a scalar function in a double space. The coordinate $\mathbf{x}_e$ refers to the position of the electron while $\mathbf{x}_h$ refers to the position of the hole. χ_S is invariant to lattice-vector shifts when applied simultaneously to $\mathbf{x}_h$ and $\mathbf{x}_e$. Due to the high dimensionality the discussion of χ is not easily possible. To get the best insight into the real-space correlation between the hole and the electron in the excited state and to observe the attractive nature of this correlation, one
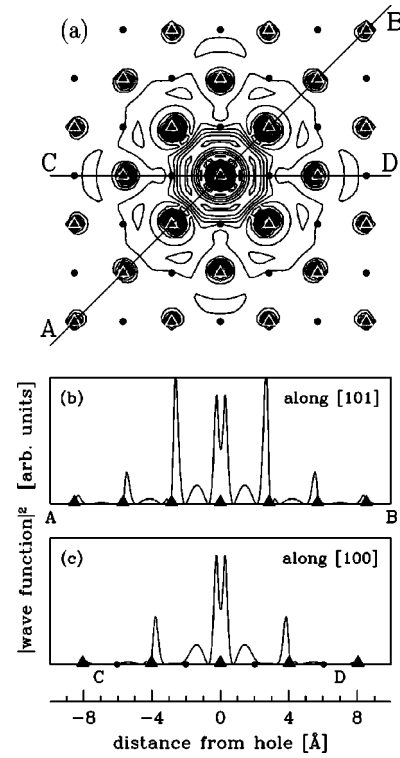

FIG. 11. (a) Real-space distribution $|\chi_S(\mathbf{x}_h, \mathbf{x}_e)|^2$ of the electron ($\mathbf{x}_e$) with respect to the hole ($\mathbf{x}_h$) for the lowest-energy exciton in LiF (at 12.8 eV), in the (010) plane. Dots (triangles) denote Li (F) atoms. The hole ($\mathbf{x}_h$) is fixed at the central F atom. (b, c) The same quantity, along the lines AB and CD indicated in panel (a).

should keep one of the particles fixed and discuss χ with respect to the coordinates of the other particle. This gives a correlation function that depends mainly on the difference, $(\mathbf{x}_e - \mathbf{x}_h)$, but includes all details of the microscopic structure of the excited state. In the case of a simplified isotropic effective-mass model, this correlation function would correspond to the envelope function of an exciton, which is given by hydrogenlike wave functions. In our present approach, however, much more detail is obtained.

As an illustration, we show in Fig. 11 the lowest-energy spin-singlet exciton in LiF (at 12.8 eV excitation energy). In panel (a) we show the distribution of the electron relative to the hole, which we fix at an F atom, in the (010) plane. The envelope function is s-like, with slight modifications due to the anisotropy of the cubic crystal, and has a mean radius of slightly over 4 Å or one lattice constant. Excitons in LiF have often been thought of as typical examples for Frenkel-like excitons, i.e., the excitation of the electron takes place at one atomic site or between neighboring atoms. Our results, however, clearly show that the exciton is larger than that. The electron distribution of the second and third exciton is similar to Fig. 11(a). Figures 11(b) and (c) show the same quantity as a line plot along the [101], as well as along the [100] direction [indicated as lines AB and CD, respectively, in panel (a)]. The figures exhibit several interesting features. First, the charge density of the electron is very low at the Li atoms. From an extreme Frenkel exciton–like picture, one might have expected that the electron hops from the central F atom to the nearest-neighbor Li atoms. Instead, it partly remains on the central F atom and partly hops to the first- and

second-nearest F atoms and even farther away. Second, the electron distribution on these neighbor F atoms is not isotropic, but is highly polarized towards the central F atom. This results from the correlation of the quasielectron to the effective positive charge of the quasihole on the central F atom.

V. CONCLUSIONS

We have presented a recently developed approach to calculate the optical spectra of real materials from first principles. This requires the evaluation of the spectrum of the single-particle and the two-particle Green's function. The electron self-energy operator, which occurs in the equation of motion of both Green's functions, is calculated within the GW approximation. From the electron-hole excitations of the two-particle Green's function and the corresponding optical transition matrix elements, the optical spectrum is calculated.

We have developed computational schemes for the first-principles application of this approach to real materials. The approach in general holds for semiconducting condensed-matter systems on all length scales, including atoms and molecules, clusters, quantum dots, polymers, surfaces, and crystals. Depending on the system, however, particular technical issues must be addressed. A number of such issues have been discussed in detail. In the particular case of periodic crystals, we have presented a novel interpolation scheme in reciprocal space that allows one to calculate the electron-hole interaction at very moderate cost.

We have discussed electron-hole excitations in atoms, molecules, and clusters (as examples for isolated systems), as well as the optical spectra of semiconductor and insulator crystals. In all cases the results are in excellent agreement with measured data. The approach can be employed to investigate both bound exciton states below and resonant excitonic states above the fundamental gap energy. The excitation energies and the spectra are drastically influenced by the electron-hole interaction, thus demonstrating the crucial role of two-particle correlation. Without the interaction, i.e., on the level of noninteracting quasiparticles, the spectra deviate significantly from the measured data.

[1] L. Hedin, Phys. Rev. **139**, A796 (1965).

[2] L. Hedin and S. Lundqvist, in *Solid State Physics, Advances in Research and Application*, edited by F. Seitz, D. Turnbull, and H. Ehrenreich (Academic, New York, 1969), Vol. 23, p. 1.

[3] M.S. Hybertsen and S.G. Louie, Phys. Rev. Lett. **55**, 1418 (1985); Phys. Rev. B **34**, 5390 (1986); S.G. Louie, in *Quantum Theory of Real Materials*, edited by J.R. Chelikowsky and S.G. Louie (Kluwer, Boston, 1996), p. 83.

[4] R.W. Godby, M. Schlüter, and L.J. Sham, Phys. Rev. Lett. **56**, 2415 (1986); Phys. Rev. B **37**, 10159 (1988).

[5] M. Rohlfing, P. Krüger, and J. Pollmann, Phys. Rev. Lett. **75**, 3489 (1995); Phys. Rev. B **52**, 1905 (1995).

[6] F. Aryasetiawan and O. Gunnarsson, Rep. Prog. Phys. **61**, 237 (1998).

[7] W.G. Aulbur, L. Jönsson, and J.W. Wilkins, in *Solid State Physics, Advances in Research and Application*, edited by H. Ehrenreich and S. Spaepen (Academic, New York, 2000), Vol. 54, p. 1.

[8] L.J. Sham and T.M. Rice, Phys. Rev. **144**, 708 (1966).

[9] G. Strinati, Phys. Rev. Lett. **49**, 1519 (1982); Phys. Rev. B **29**, 5718 (1984); Riv. Nuovo Cimento **11**, 1 (1988).

[10] W. Hanke and L.J. Sham, Phys. Rev. Lett. **43**, 387 (1979); Phys. Rev. B **21**, 4656 (1980).

[11] M. Rohlfing and S.G. Louie, Phys. Rev. Lett. **80**, 3320 (1998); **81**, 2312 (1998); **82**, 1959 (1999); **83**, 856 (1999); Phys. Status Solidi A **175**, 17 (1999).

[12] G. Onida, L. Reining, R.W. Godby, R. Del Sole, and W. Andreoni, Phys. Rev. Lett. **75**, 818 (1995).

[13] S. Albrecht, G. Onida, and L. Reining, Phys. Rev. B **55**, 10 278 (1997); S. Albrecht, L. Reining, R. Del Sole, and G. Onida, Phys. Rev. Lett. **80**, 4510 (1998); Phys. Status Solidi A **170**, 189 (1998).

[14] L.X. Benedict, E.L. Shirley, and R.B. Bohn, Phys. Rev. Lett. **80**, 4514 (1998); Phys. Rev. B **57**, R9385 (1998); *ibid.* **59**, 5441 (1999).

[15] J.-W. van der Horst, P.A. Bobbert, M.A.J. Michels, G. Brooks, and P.J. Kelly, Phys. Rev. Lett. **83**, 4413 (1999).

[16] R. Del Sole and E. Fiorino, Phys. Rev. B **29**, 4631 (1984).

[17] The generalization of the approach to open-shell systems, as well as, the incorporation of spin-orbit interaction via appropriate additional pseudopotentials, is straightforward. These generalizations require, however, that the spin be explicitly taken into account as an additional degree of freedom. This doubles the subspace of single-particle states to be considered, and the basis for electron-hole excitations is increased by a factor of 4. The classification of excitations as spin-singlet and -triplet transitions is then no longer possible.

[18] In the case of gap-free systems, i.e., for extended metals, the electron-hole interaction is in general not significant due to the metallic screening, and excitonic effects are not dominant in the optical properties. Thus the optical spectrum can in most cases already be discussed on the level of the one-body Green's function.

[19] G.B. Bachelet, D.R. Hamann, and M. Schlüter, Phys. Rev. B **26**, 4199 (1982).

[20] This is distinctly different from the corresponding expressions within time-dependent density-functional theory (TDDFT). In TDDFT, both the diagonal and the off-diagonal blocks are of the

same order of magnitude, and the off-diagonal blocks cannot be neglected.

[21] A. Fetter and J.D. Walecka, *Quantum Theory of Many Particle Systems* (McGraw-Hill, San Francisco, 1971), p. 538.

[22] Including the functional derivative $\partial W / \partial G_1$ in the formalism would drastically increase its complexity. It is, unfortunately, difficult to estimate the influence of this term. Although Strinati argues that it should not be very important for extended systems (Ref. 9), the use of this approximation is only justified by its success.

[23] B. Adolph, V.I. Gavrilenko, K. Tenelsen, F. Bechstedt, and R. Del Sole, Phys. Rev. B **53**, 9797 (1996).

[24] Z.H. Levine and D.C. Allan, Phys. Rev. Lett. **63**, 1719 (1989); Phys. Rev. B **43**, 4187 (1991).

[25] H.N. Rojas, R.W. Godby, and R.J. Needs, Phys. Rev. Lett. **74**, 1827 (1995); M.M. Rieger, L. Steinbeck, I.D. White, H.N. Rojas, and R.W. Godby, Comput. Phys. Commun. **117**, 211 (1999).

[26] E. Runge and E.K.U. Gross, Phys. Rev. Lett. **52**, 997 (1984); M. Petersilka, U.J. Gossmann, and E.K.U. Gross, *ibid.* **76**, 1212 (1996).

[27] R. Bauernschmitt and R. Ahlrichs, Chem. Phys. Lett. **256**, 454 (1996).

[28] E.L. Shirley and R.M. Martin, Phys. Rev. B **47**, 15 404 (1993); **47**, 15 413 (1993).

[29] *Numerical Data and Functional Relationships in Science in Technology* (Springer, Berlin, 1950), Vol. I, part 1.

[30] U. Itoh, Y. Toyoshima, and H. Onuki, J. Chem. Phys. **85**, 4867 (1986).

[31] See, e.g., H. Takagi *et al.*, Appl. Phys. Lett. **56**, 2379 (1990); C. Delerue, G. Allan, and M. Lannoo, Phys. Rev. B **48**, 11 204 (1993); A. Francheschetti and A. Zunger, Phys. Rev. Lett. **78**, 915 (1997); S. Öğüt, J.R. Chelikowsky, and S.G. Louie, *ibid.* **79**, 1770 (1997).

[32] D.E. Aspnes and A.A. Sturge, Phys. Rev. B **27**, 985 (1983).

[33] P. Lautenschlager, M. Garriga, S. Logothetidis, and M. Cardona, Phys. Rev. B **35**, 9174 (1987).

[34] H.R. Philipp, J. Appl. Phys. **43**, 2836 (1972); D.E. Aspnes and J.B. Theeten, J. Electrochem. Soc. **127**, 1359 (1980).

[35] P. Lautenschlager, M. Garriga, L. Viña, and M. Cardona, Phys. Rev. B **36**, 4821 (1987).

[36] D.M. Roessler and W.C. Walker, J. Opt. Soc. Am. **57**, 835 (1967).

[37] G. Baldini and B. Bosacchi, Phys. Status Solidi **38**, 325 (1970).